iScience

CellPress
OPEN ACCESS

Article

# Synaptic scaling of corticostriatal circuits underlies hyperactivity in GABA Transporter-1 deficient mice

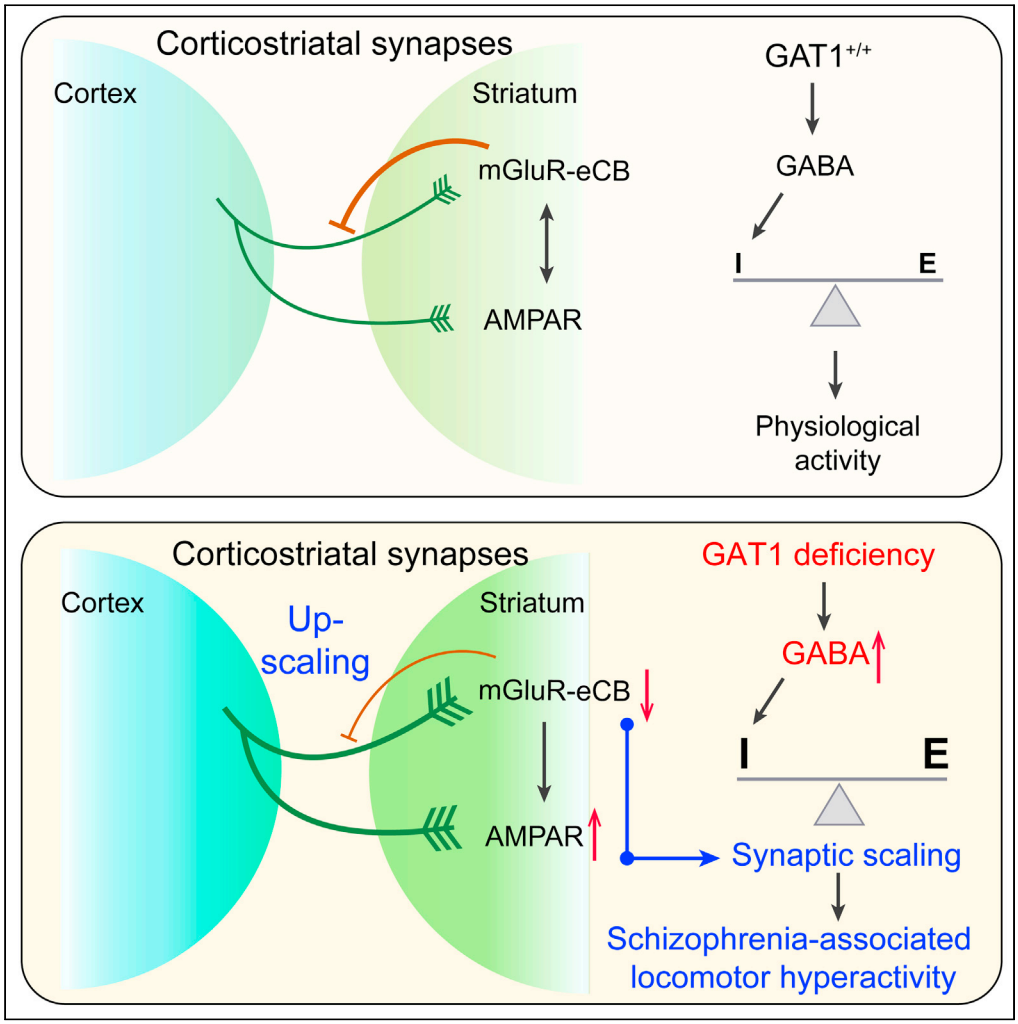


Yan-Jiao Wu, Xin Yi, Xue Gu, ..., Jianqing Ding, Wei-Guang Li, Tian-Le Xu

jqding18@yahoo.com (J.D.)
liwg@fudan.edu.cn (W.-G.L.)
xu-happiness@shsmu.edu.cn (T.-L.X.)

## Highlights

Elevated ambient GABA causes an increase in striatal excitatory transmission

GAT1 deficiency results in upregulation of striatal homomeric-GluA1 AMPARs

Impaired mGluR-eCB underlies corticostriatal enhancement in GAT1$^{-/-}$ mice

Correction of excitatory transmission reverses hyperactivity in GAT1$^{-/-}$ mice

Wu et al., iScience 26, 106322
April 21, 2023 
https://doi.org/10.1016/j.isci.2023.106322

iScience

CellPress
OPEN ACCESS

Article

# Synaptic scaling of corticostriatal circuits underlies hyperactivity in GABA Transporter-1 deficient mice

Yan-Jiao Wu,[1,2,7] Xin Yi,[1,2,3,7] Xue Gu,[1,2] Qi Wang,[1,2] Qin Jiang,[1,2] Ying Li,[1,2] Michael X. Zhu,[4] Jianqing Ding,[5,*] Wei-Guang Li,[2,3,6,*] and Tian-Le Xu[1,2,6,8,*]

## SUMMARY

**Homeostatic synaptic scaling entails adjustment of synaptic strength on a cell to prolonged changes of neuronal activity, which is postulated to participate in neuropsychiatric disorders *in vivo*. Here, we find that sustained elevation in ambient GABA levels, by either genetic deletion or pharmacological blockade of GABA transporter-1 (GAT1), leads to synaptic scaling up of corticostriatal pathways, which underlies locomotor hyperactivity. Meanwhile, medium spiny neurons of the dorsal striatum exhibit an aberrant increase in excitatory synaptic transmission and corresponding structural changes in dendritic spines. Mechanistically, GAT1 deficiency dampens the expression and function of metabotropic glutamate receptors (mGluRs) and endocannabinoid (eCB)-dependent long-term depression of excitatory transmission. Conversely, restoring mGluR function in GAT1 deficient mice rescues excitatory transmission. Lastly, pharmacological potentiation of mGluR-eCB signaling or inhibition of homomeric-GluA1 AMPA receptors eliminates locomotor hyperactivity in the GAT1 deficient mice. Together, these results reveal a synaptic scaling mechanism in corticostriatal pathways that regulate locomotor activity.**

## INTRODUCTION

Homeostatic remodeling at the synaptic and circuit levels keeps the central nervous system in a steady state to prevent overactivity and underactivity, thus crucial for fine-tuning the network excitability across space and time.[1–3] Synaptic scaling refers to a phenomenon in which perturbing network activity can produce compensatory and counterproductive changes to reverse activity to baseline values, which is initially discovered in cultured neocortical neurons.[4–7] Synaptic scaling provides such a type of homeostasis by adjusting the strength of synapses globally or specifically upward or downward to stabilize the firing of a neuron.[8–10] This form of homeostatic synaptic plasticity is thought to be crucial for processes ranging from learning and memory[11,12] to activity-dependent development.[13,14] Pathologically, homeostatic plasticity has been hypothesized to be involved in a variety of neuropsychiatric disorders with excitation-inhibition (E-I) imbalance, but the mechanisms remain not well understood. Therefore, it is important to determine the molecular and cellular mechanisms underlying the synaptic scaling, as well as compensatory changes because of inadequate or maladaptive homeostatic remodeling of specific circuits, which have a significant impact on animal behavior in health and pathological conditions.[15–17]

The abnormality of the GABA system has increasingly emerged as a major confluence of genetic and environmental susceptibility factors for schizophrenia.[3,18,19] Solute carrier family 6 member 1 (SLC6A1) encodes GABA transporter-1 (GAT1), a key transporter responsible for removal of GABA from the synaptic cleft and termination of GABAergic neurotransmission. GAT1 is highly expressed in the olfactory bulb, neocortex, cerebellum, basal ganglia, and glial cells[20–22] and significantly reduced in schizophrenia patients.[23] In addition, missense damaging *de novo* variants of the gene encoding GAT1 also confer a very high risk of schizophrenia[24] and several other neurodevelopmental phenotypes.[25–29] Our previous studies showed that the GAT1 knockout ($GAT1^{-/-}$) mice had elevated ambient GABA levels in the brain, and displayed multiple behavioral abnormalities that closely resemble schizophrenic positive, negative, and cognitive symptoms.[30,31] Thus, $GAT1^{-/-}$ mice were validated as an animal model of psychosis and

[1]Songjiang Hospital and Songjiang Research Institute, Shanghai Jiao Tong University School of Medicine, Shanghai 201600, China

[2]Department of Anatomy and Physiology, Shanghai Jiao Tong University School of Medicine, Shanghai 200025, China

[3]Department of Rehabilitation Medicine, Huashan Hospital, Institute for Translational Brain Research, State Key Laboratory of Medical Neurobiology and Ministry of Education Frontiers Center for Brain Science, Fudan University, Shanghai 200032, China

[4]Department of Integrative Biology and Pharmacology, McGovern Medical School, University of Texas Health Science Center at Houston, Houston, TX 77030, USA

[5]Institute of Aging and Tissue Repair, Ren Ji Hospital, Shanghai Jiao Tong University School of Medicine, Shanghai 200127, China

[6]Shanghai Research Center for Brain Science and Brain-Inspired Intelligence, Shanghai 201210, China

[7]These authors contributed equally

[8]Lead contact

*Correspondence: jqding18@yahoo.com (J.D.), liwg@fudan.edu.cn (W.-G.L.), xu-happiness@shsmu.edu.cn (T.-L.X.)

https://doi.org/10.1016/j.isci.2023.106322

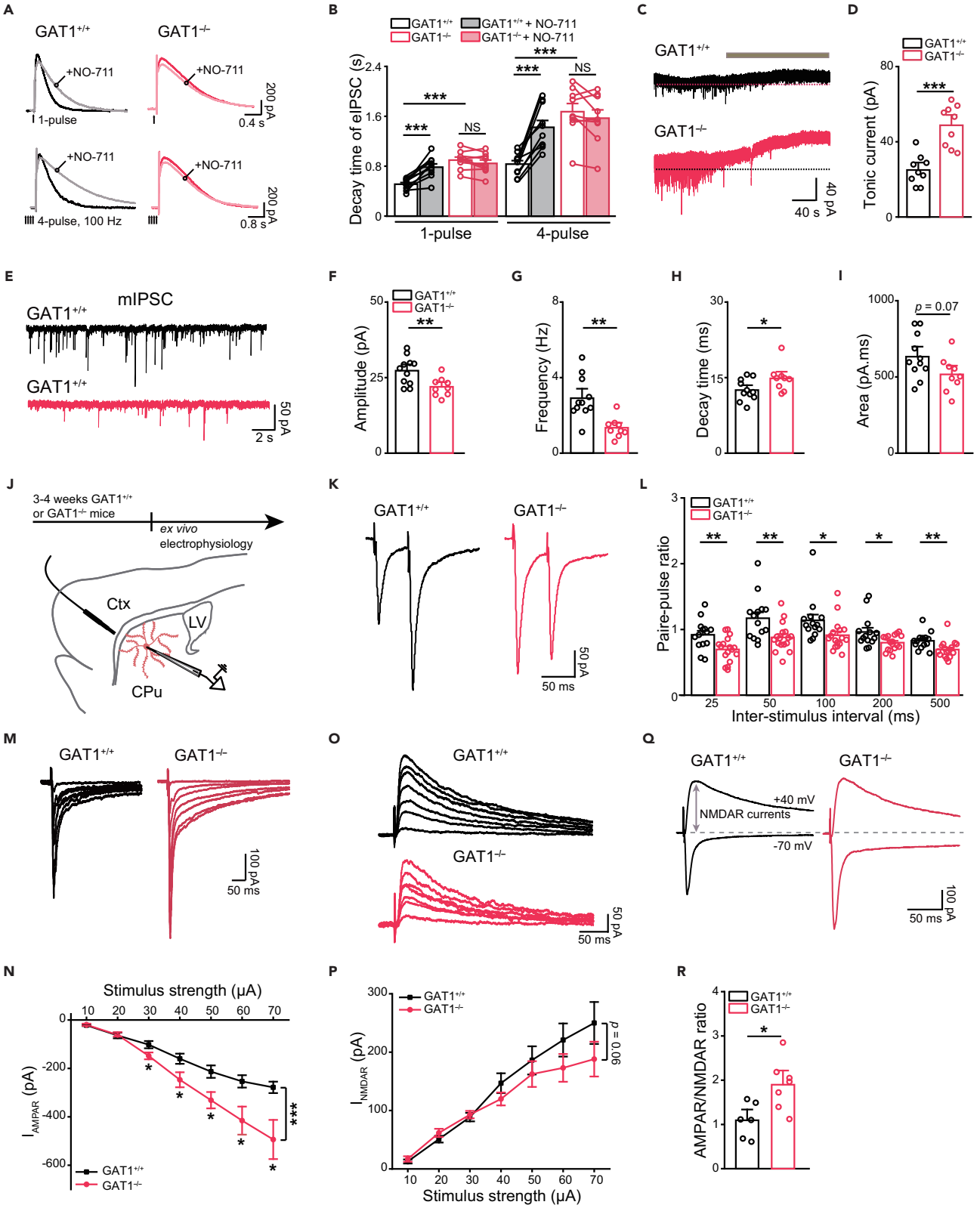
A
GAT1+/+
GAT1−/−
+NO-711
1-pulse
200 pA
0.4 s
4-pulse, 100 Hz
0.8 s
B
GAT1+/+
GAT1−/−
GAT1+/+ + NO-711
GAT1−/− + NO-711
Decay time of eIPSC (s)
NS
1-pulse
4-pulse
C
GAT1+/+
GAT1−/−
40 pA
40 s
D
Tonic current (pA)
E
mIPSC
GAT1+/+
50 pA
2 s
F
Amplitude (pA)
G
Frequency (Hz)
H
Decay time (ms)
I
Area (pA.ms)
p = 0.07
J
3-4 weeks GAT1+/+
or GAT1−/− mice
ex vivo
electrophysiology
Ctx
LV
CPu
K
50 pA
50 ms
L
Paire-pulse ratio
Inter-stimulus interval (ms)
M
100 pA
50 ms
O
Q
+40 mV
NMDAR currents
-70 mV
N
Stimulus strength (μA)
I AMPAR (pA)
P
I NMDAR (pA)
p = 0.06
R
AMPAR/NMDAR ratio

**Figure 1. Characterization of striatal inhibitory and excitatory synaptic transmission in the GAT1$^{-/-}$ mice**

(A and B) Decay time of electrical stimulation-evoked inhibitory postsynaptic currents (eIPSCs) of MSNs in dorsal striatum. (A) Representative eIPSC traces. (B) Quantification of decay time of 1-pulse and 4-pulse (100 Hz) compound eIPSCs before and after bath application of NO-711 (10 μM). GAT1$^{+/+}$ versus GAT1$^{-/-}$, unpaired Student's *t* test; GAT1$^{+/+}$ versus GAT1$^{+/+}$ + NO-711, GAT1$^{-/-}$ versus GAT1$^{-/-}$ + NO-711, paired Student's *t* test, n = 10 neurons from four GAT1$^{+/+}$ mice and n = 9 neurons from three GAT1$^{-/-}$ mice.

(C and D) Tonic GABA currents. Unpaired Student's *t* test, n = 9 neurons from four GAT1$^{+/+}$ mice and n = 9 neurons from five GAT1$^{-/-}$ mice.

(E–I) Miniature inhibitory postsynaptic currents. Unpaired Student's *t* test, n = 11 neurons from three GAT1$^{+/+}$ mice and n = 9 neurons from four GAT1$^{-/-}$ mice.

(J–L) PPRs at the corticostriatal projections. (J) Experimental schemes. Ctx, cortex; LV, lateral ventricle; CPu, caudate putamen (dorsal striatum). (K) Representative traces showing paired-pulse responses with 50-ms interval. (L) Statistics of PPRs. Unpaired Student's *t* test, n = 14 neurons from six GAT1$^{+/+}$ mice and n = 17 neurons from five GAT1$^{-/-}$ mice.

(M–P) AMPAR (M and N) and NMDAR (O and P)-mediated synaptic currents evoked by electrical stimuli of different intensities at the corticostriatal projections. (M and O) Representative traces. (N) I-O relationship of AMPAR-mediated currents. Unpaired Student's *t* test and two-way repeated measures ANOVA, main effects of genotype, $F_{1,161} = 25.802$, $p < 0.001$, n = 12 neurons from three GAT1$^{+/+}$ mice and n = 11 neurons from three GAT1$^{-/-}$ mice. (P) I-O relationship of NMDAR-mediated currents. Two-way repeated measures ANOVA, main effects of genotype, $F_{1,134} = 3.618$, $p = 0.06$, n = 11 neurons from three GAT1$^{+/+}$ mice and n = 8 neurons from three GAT1$^{-/-}$ mice.

(Q and R) AMPAR/NMDAR ratios at the corticostriatal synapses. Unpaired Student's *t* test, n = 6 neurons from two GAT1$^{+/+}$ mice and n = 7 neurons from two GAT1$^{-/-}$ mice.

Data are represented as mean ± SEM. *, $p < 0.05$, **, $p < 0.01$, ***, $p < 0.001$, NS, no significant significance.

neurodevelopmental disorders exhibiting typical schizophrenia-like phenotypes.[18,32] As a result, $GABA_A$ receptor antagonist picrotoxin (PTX) effectively ameliorated the behavioral defects in the GAT1$^{-/-}$ mice, supporting the pathological nature of the E-I imbalance.[31] These genetic and pharmacological studies beg for two important questions: Does elevation of GABA drive homeostatic synaptic scaling of excitatory synaptic transmission *in vivo*? Is homeostatic scaling driven by E-I imbalance involved in the manifestation of behavioral symptoms in schizophrenia?

As most of the previous mechanistic studies on synaptic scaling have been conducted on the neocortical or hippocampal pyramidal neurons, whether the mechanisms underlying synaptic scaling *in vivo* and other brain regions are similar or distinct remain an open question. In the current study, we employed the GAT1$^{-/-}$ mice as a mouse model of schizophrenia, to dissect the roles of homeostatic plasticity in the schizophrenia-associated symptoms. Together with the use of prolonged pharmacological inhibition of GAT1 activity from weaning to induce locomotion hyperactivity in wild type mice, we identified homeostatic synaptic scaling in the corticostriatal pathway to be crucial for conferring the behavioral phenotype of locomotor hyperactivity associated with GAT1 disruption. We provide genetic and pharmacological evidence that counteracting such synaptic scaling represents a potential therapeutic strategy to mitigate the behavioral phenotype.

## RESULTS

### Scaling up of corticostriatal excitatory synaptic transmission in GAT1$^{-/-}$ mice

Dysregulation of corticostriatal circuitry is thought to be critical for psychotic locomotor hyperactivity, a positive symptom in schizophrenia.[33–35] Aiming for early adult-onset schizophrenia,[36] we focused our analysis on young mice (3–5 weeks), which mimic early adolescence in humans.[37] GAT1 is highly expressed in the striatum,[21,22,38–40] but whether and how E-I imbalance there because of GAT1 deficiency[41] contributes to locomotor hyperactivity[31] remained unexplored. To fill this gap, we first examined the effect of GAT1 disruption on GABAergic transmission by using whole-cell recording of MSNs in acute brain slices. MSNs have densely spinous dendrites and are the most abundant neuronal type in the striatum.[42] Inhibitory postsynaptic currents (IPSCs) were evoked by single-pulse electrical stimulation within the dorsal striatum by clamping the patched MSNs at 0 mV, the reversal potential of glutamate receptor-mediated cationic currents. We measured $GABA_A$R-mediated electrically evoked IPSCs (eIPSCs) in response to different electrical stimulus intensities (input-output curve, I-O curve) and observed a slight but significant decrease in the amplitudes of eIPSCs in the GAT1$^{-/-}$ compared to GAT1$^{+/+}$ mice (Figures S1A and S1B). Notably, the decay time of the eIPSCs in slices from GAT1$^{-/-}$ mice was longer than that from GAT1$^{+/+}$ mice. Moreover, inhibition of GAT1 activity by NO-711 (10 μM) also extended the delay time of eIPSC in GAT1$^{+/+}$, but not GAT1$^{-/-}$ slices (Figures 1A and 1B). A burst stimulation containing 4 pulses at 100 Hz elicited compound eIPSCs that exhibited a markedly longer decay time than the single eIPSCs. NO-711 further prolonged the burst-induced compound eIPSCs in GAT1$^{+/+}$ but not GAT1$^{-/-}$ slices (Figures 1A and 1B). NO-711 decreased the amplitude of the burst-induced compound eIPSCs in GAT1$^{+/+}$ but not GAT1$^{-/-}$ slices, and did not affect that of the single eIPSCs in GAT1$^{+/+}$ and GAT1$^{-/-}$ slices (Figure S1C). We then evaluated the function of astrocyte-specific GABA transporter-3 (GAT3)[43] in the GAT1$^{-/-}$ mice. Indeed, in both GAT1$^{+/+}$ and GAT1$^{-/-}$ mice, blocking GAT3 with

SNAP5114 (40 μM) resulted in a significantly prolonged decay time of eIPSCs, although their amplitudes were also reduced (Figures S2A–S2C). Quantification of the SNAP5114-induced changes in decay time showed that the GAT3 activity was upregulated in the GAT1$^{-/-}$ compared to GAT1$^{+/+}$ mice (Figure S2D), implying that the ambient GABA levels were enhanced in the GAT1$^{-/-}$ mice.

To further probe the impacts of GAT1 deficiency on striatal GABAergic inhibition, we compared the tonic and phasic GABA currents between GAT1$^{+/+}$ and GAT1$^{-/-}$ slices. Of note, GAT1 knock out significantly potentiated the tonic currents (Figures 1C and 1D). By contrast, the phasic GABA currents, as revealed by miniature IPSCs (mIPSCs), exhibited decreases in amplitude, frequency, and current area, but an increase in the decay time in GAT1$^{-/-}$ slices (Figures 1E–1I). Together, these results indicate that disruption of GAT1-mediated GABA uptake alters GABAergic transmission by prolonging the time course of GABA action.

Given the altered GABAergic transmission in GAT1$^{-/-}$ mice, we asked whether homeostatic synaptic scaling occurred at the corticostriatal excitatory projections in these animals. To measure the synaptic strength of corticostriatal projections in the GAT1$^{-/-}$ mice, we recorded electrically evoked EPSCs (eEPSCs) in MSNs of the dorsal striatum by stimulation of the corpus callosum, which preferentially activates cortical afferents to MSNs (Figure 1J). With paired electrical pulses at varying inter-stimulus intervals, we measured the paired-pulse ratios (PPRs) of eEPSCs, which were inversely related to the presynaptic release probability.[44] The PPRs were significantly decreased in the GAT1$^{-/-}$ compared to GAT1$^{+/+}$ mice, suggesting that presynaptic release probability was enhanced in corticostriatal synapses of the GAT1$^{-/-}$ mice (Figures 1K and 1L). Moreover, by holding the patched MSNs at either −70 or +40 mV, we measured AMPAR- and NMDAR-mediated eEPSCs, respectively, in response to different electrical stimulus intensities to determine the activity of AMPAR and NMDAR in corticostriatal synapses (I-O curve). We observed prominent increases in the amplitudes of AMPAR-mediated eEPSCs in GAT1$^{-/-}$ compared to GAT1$^{+/+}$ mice at most of the stimulus intensities used (Figures 1M and 1N). However, the amplitudes of NMDAR-mediated eEPSCs only showed a marginal decrease in the GAT1$^{-/-}$ mice, which did not reach statistical significance (Figures 1O and 1P). Further analysis revealed a significant increase in the AMPAR/NMDAR ratios in the GAT1$^{-/-}$ mice (Figures 1Q and 1R). These results suggest that accompanying the altered GABAergic transmission in the GAT1$^{-/-}$ mice, the corticostriatal excitatory synapses scale up, which presumably counteracts the continuous elevation of ambient GABA levels in this mouse model.

## Prolonged pharmacological blockade of GAT1 activity recapitulates the scaling up of corticostriatal excitatory synaptic transmission as that seen in GAT1$^{-/-}$ mice

To strengthen the effects of GAT1 disruption on homeostatic excitatory synaptic scaling, we subjected wild type mice to NO-711 via drinking water from weaning (~3 weeks old) for ten days in the adolescent stage for prolonged *in vivo* pharmacological blockade of GAT1 activity (Figure 2A). We determined the concentration of NO-711 by high-performance liquid chromatography mass spectrometry (LC-MS). We found the concentrations of NO-711 in the brain up to 10 ng/g after a single day administration via drinking water (Figure S3A), which was consistent with the idea that NO-711 can cross the blood-brain barrier as a potent anticonvulsant compound.[45] Behaviorally, mice chronically treated with NO-711 exhibited locomotor hyperactivity compared to the vehicle-treated mice, resembling the phenotype of the GAT1$^{-/-}$ mice (Figures S3B–S3E). In whole-cell slice recordings of the synaptic activity in the corticostriatal pathways, we found a significant reduction of PPRs in NO-711- compared to vehicle-treated mice, suggesting that GAT1 inhibition causes an enhancement of presynaptic release probability in the corticostriatal synapses (Figures 2B and 2C). We then measured AMPAR- and NMDAR-mediated eEPSCs of MSNs by holding at −70 mV and +40 mV, respectively, in response to different electrical stimulus intensities of the corticostriatal projections. We observed a prominent increase in the amplitudes of AMPAR-, but not NMDAR-, mediated eEPSCs (Figures 2D–2G), as well as an increase in the AMPAR/NMDAR ratios (Figures 2H and 2I), in the NO-711-treated mice, similar to that observed in the GAT1$^{-/-}$ mice. These results indicate that prolonged pharmacological blockade of GAT1 activity *in vivo* has similar effects on homeostatic synaptic scaling at the corticostriatal pathways and locomotor hyperactivity as genetic ablation of the GAT1 gene.

## Loss of GAT1 results in aberrant maturation of striatal excitatory synapses

To further characterize the effect of GAT1 disruption on synaptic scaling, we next analyzed the morphological and functional changes of excitatory synapses formed on MSNs. By Golgi staining, we traced MSNs and compared spine morphology and spine density between GAT1$^{+/+}$ and GAT1$^{-/-}$ mice. The results revealed a significant increase in spine head width, but a decrease in spine density in the GAT1$^{-/-}$ mice

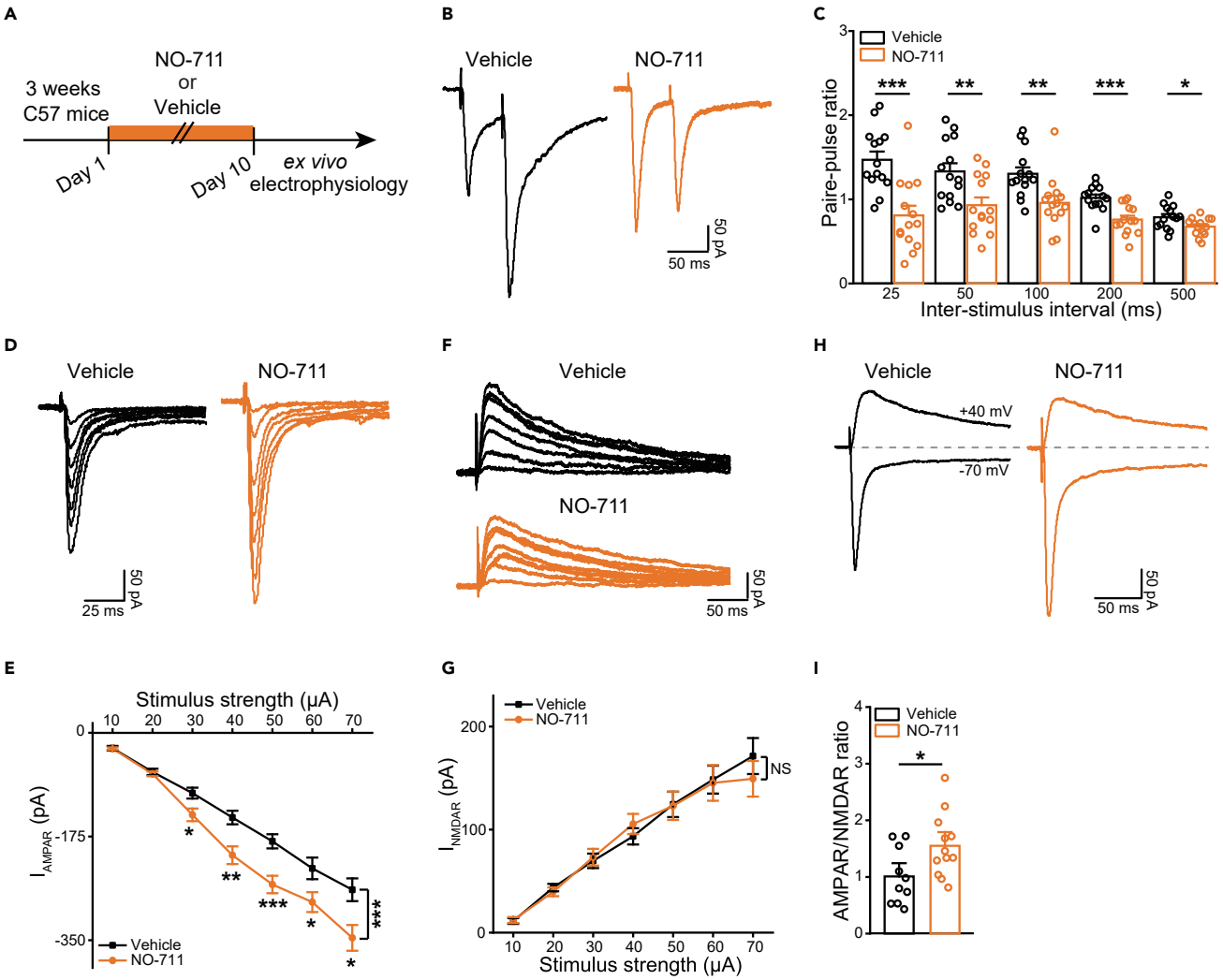


**Figure 2. Prolonged pharmacological blockade of GAT1 activity recapitulates the scaling up of corticostriatal excitatory synaptic transmission as that seen in the GAT1$^{-/-}$ mice**

(A–C) Effects of chronic GAT1 blockade on PPRs of eEPSCs at the corticostriatal pathway. (A) Experimental scheme. (B) Representative traces showing paired-pulse responses with 50-ms interval. (C) Statistics of PPRs. Unpaired Student's *t* test, Vehicle group, n = 14 neurons from eight mice; NO-711 group, n = 14 neurons from eight mice.

(D–G) Effects of GAT1 blockade on AMPAR (D and E) and NMDAR (F and G)-mediated synaptic currents. (D and F) Representative traces. (E) I-O relationship of AMPAR-mediated currents. Unpaired Student's *t* test and two-way repeated measures ANOVA, main effects of NO-711, $F_{1,189} = 40.483$, $p < 0.001$, Vehicle group, n = 13 neurons from seven mice; NO-711 group, n = 17 neurons from eight mice. (G) I-O relationship of NMDAR-mediated currents. Two-way repeated measures ANOVA, main effects of NO-711, $F_{1,126} = 0.115$, $p = 0.735$, Vehicle group, n = 10 neurons from five mice; NO-711 group, n = 8 neurons from five mice.

(H and I) Effects of chronic GAT1 blockade on AMPAR/NMDAR ratios. Unpaired Student's *t* test, Vehicle group, n = 10 neurons from three mice; NO-711 group, n = 12 neurons from three mice.

Data are represented as mean ± SEM. *, $p < 0.05$, **, $p < 0.01$, ***, $p < 0.001$, NS, no significant significance.

(Figures 3A–3C). Upon more detailed analysis of the spine morphology, we found an increase in the percentage of mushroom spines, a decrease in the percentage of filopodia spines, and no change in the percentage of stubby spines in the GAT1$^{-/-}$ mice (Figure 3D). The mushroom spines represent more mature excitatory synapses, whereas the stubby and filopodia spines represent immature synapses.[46,47] Therefore, it is possible that the loss of GAT1 promotes synaptic maturation (increased number of mushroom spines), which could be accompanied with a decrease in the overall spine density in the striatum beacuse of developmental pruning of immature spines (stubby spines and filopodia). To test this hypothesis, we analyzed the size of postsynaptic density (PSD) in the striatum using electron microscopy (EM). PSD

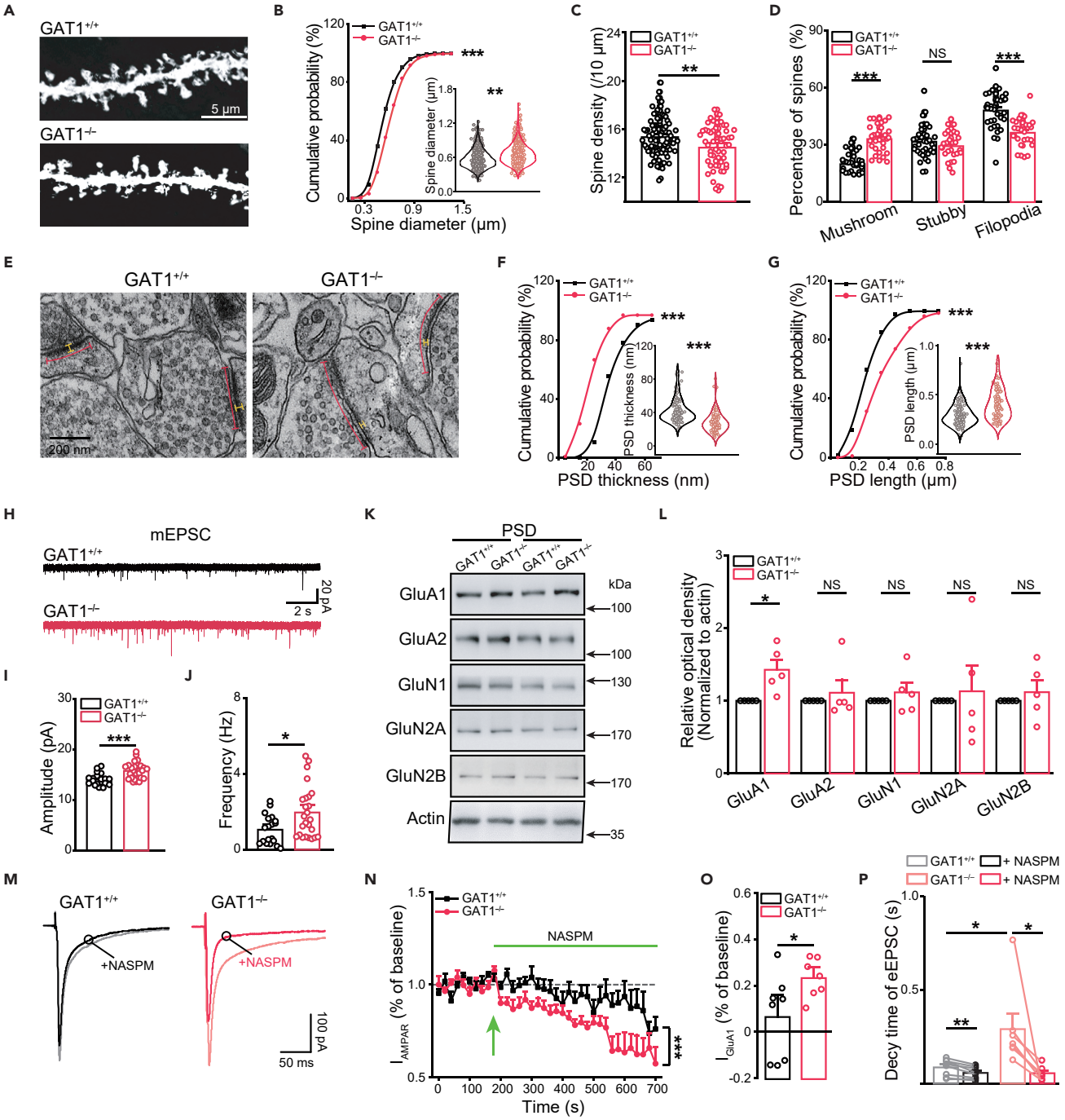


**Figure 3. Loss of GAT1 results in aberrant maturation of striatal excitatory synapses**

(A–D) Dendritic spine morphology of MSNs by Golgi staining. (A) Representative micrographs. Scale bar, 5 µm. (B) Cumulative and violin plots of spine head width. Two-sample Kolmogorov-Smirnov test and unpaired Student's *t* test, n = 2178 spines from three GAT1$^{+/+}$ mice and n = 2145 spines from three GAT1$^{-/-}$ mice. (C and D) Quantification of spine density (C) and percentage of different spine subtypes (D). Unpaired Student's *t* test, n = 73 dendritic segments from three GAT1$^{+/+}$ mice and n = 81 dendritic segments from three GAT1$^{-/-}$ mice.

(E–G) PSD morphology in the striatum by EM. (E) Representative electron micrographs depicting synaptic contacts and PSDs. (F and G) Quantification of PSD thickness (F) and length (G). Two-sample Kolmogorov-Smirnov test and unpaired Student's *t* test, n = 133 PSDs from three GAT1$^{+/+}$ mice and n = 99 PSDs from three GAT1$^{-/-}$ mice.

(H–J) Miniature excitatory postsynaptic currents of MSNs. Unpaired Student's *t* test, n = 19 neurons from four GAT1$^{+/+}$ mice and n = 25 neurons from six GAT1$^{-/-}$ mice.

**Figure 3. *Continued***

(K and L) Immunoblots of GluA1, GluA2, GluN1, GluN2A and GluN2B in the purified PSD fractions of striatum. Each circle denotes an individual sample (each sample prepared by pooling striata from 3 mice). Unpaired Student's *t* test, n = 5 samples for each group.

(M–P) eEPSCs mediated by homomeric-GluA1 AMPARs. (M) Representative traces. (N) Time courses of eEPSCs amplitudes before and after bath application of NASPM. Two-way repeated-measures ANOVA, main effects of genotype, $F_{1,390} = 82.446$, $p < 0.001$. (O) Quantification of homomeric GluA1-mediated eEPSCs, based on current at 5 min after NASPM application normalized to the baseline. (P) Quantification of decay time of eEPSCs before and after NASPM application. Unpaired Student's *t* test, n = 8 neurons from three $GAT1^{+/+}$ mice and n = 7 neurons from three $GAT1^{-/-}$ mice.

Data are represented as mean ± SEM. *, $p < 0.05$, **, $p < 0.01$, ***, $p < 0.001$, NS, no significant significance.

is an electron-dense structure located at the spine head, which consists of densely packed ion channels, surface receptors, as well as cytoplasmic scaffolding and signaling proteins.[48] Of interest, compared to $GAT1^{+/+}$ mice, $GAT1^{-/-}$ mice had reduced PSD thickness but significantly increased PSD length (Figures 3E–3G), which the latter could underlie the increased spine width observed in Golgi staining (Figures 3A–3D). The reduced PSD thickness could result from insufficient supplies and/or time for PSD proteins to build up because of synapse overgrowth as a consequence of elevated ambient GABA in the $GAT1^{-/-}$ mice. The changes in spine density and morphology of MSNs prompted us to evaluate the glutamatergic synaptic transmission by electrophysiological recording of miniature EPSCs (mEPSCs) in striatal MSNs. We found that both the amplitude and frequency of mEPSCs were increased in the $GAT1^{-/-}$ mice (Figures 3H–3J). These results implicate an overall enhancement of striatal excitatory transmission with the loss of GAT1.

In parallel with the morphological and functional changes, we found a significant increase in the expression of GluA1, but not other glutamate receptor subunits, in PSDs of the $GAT1^{-/-}$ mice, by western blotting using biochemically purified PSDs from the striatum (Figures 3K and 3L). However, GluA1 levels in the total striatal tissues were not changed (Figures S4 and S5), indicating that the loss of GAT1 increases the postsynaptic localization of the GluA1 subunits. Plausibly, this suggests a selective increase of the homomeric-GluA1 AMPARs, or GluA2-lacking $Ca^{2+}$-permeable AMPARs (CP-AMPARs),[49] which were first identified in culture neurons and were thought to be critical for homeostatic synaptic scaling caused by suppression of synaptic activity.[50–54] To test this possibility, we recorded eEPSCs in the corticostriatal pathways of $GAT1^{+/+}$ and $GAT1^{-/-}$ mice in the absence and presence of 1-Naphthylacetyl spermine (NASPM, 50 μM), a selective CP-AMPAR antagonist. We found that NASPM inhibited eEPSCs to more extent in the $GAT1^{-/-}$ mice than in $GAT1^{+/+}$ mice (Figures 3M–3O), supporting the idea that the $GAT1^{-/-}$ mice have increased homomeric-GluA1 AMPARs in the PSD. Because different subtypes of AMPAR exhibit distinct channel kinetics, for example, CP-AMPARs lacking GluA2 subunits decay much more slowly than AMPARs containing GluA2,[55] we subsequently measured the decay time of eEPSCs at corticostriatal pathways. The decay time was significantly prolonged in $GAT1^{-/-}$ mice compared with $GAT1^{+/+}$ mice and was reduced by the NASPM inhibition (Figure 3P), which echoed the above-mentioned upregulation of GluA1 subunits and the increase of GluA2-lacking CP-AMPARs at corticostriatal pathways in the $GAT1^{-/-}$ mice. These results indicate that the scaling up of corticostriatal transmission in $GAT1^{-/-}$ mice is accompanied with corresponding changes in spine morphology, PSD components, and activity of excitatory synapses in MSNs, which may underlie hyperactivity of the striatum.

## Gene profile changes in striatum of the $GAT1^{-/-}$ mice

To explore the potential mediators of corticostriatal synaptic scaling in $GAT1^{-/-}$ mice, whole-tissue mRNA sequencing was carried out for the dorsal striatum of $GAT1^{+/+}$ and $GAT1^{-/-}$ mice. We verified that *Gat1* was the most abundant isoform of the GAT family in striatal preparations from $GAT1^{+/+}$ mice but absent in that from $GAT1^{-/-}$ mice (Figure S6). Differential expression analysis of the results revealed a subset of genes related to synaptic receptor signaling and remodeling to be specially downregulated in the $GAT1^{-/-}$ mice [233 genes with $p < 0.05$, among which 92 with $p < 0.01$, false discovery rate (FDR) adjusted] (Figure 4A). These included several subunits of mGluRs and their associated postsynaptic scaffolding proteins, e.g., Homer1, as well as components for the endocannabinoid (eCB) signaling cascades (Figure 4B), which are well known to play key roles in striatal plasticity and basal ganglia circuit function.[56–60]

Using quantitative polymerase chain reaction (qPCR) assays, we verified the decreases in the expression of mRNAs coding for enzymes in the biosynthetic pathways for eCBs, such as *Abhd4*, but not *Napepld4*, which contribute to the synthesis of anandamide (AEA), and *Daglα*, but not *Daglβ*, which contribute to the synthesis of arachidonoylglycerol (2-AG), in the striatum of the $GAT1^{-/-}$ mice. Meanwhile, the mRNA encoding the eCB receptor, *Cn1r*, but not the mRNA encoding the AEA hydrolysis enzyme, *Faah*, was also

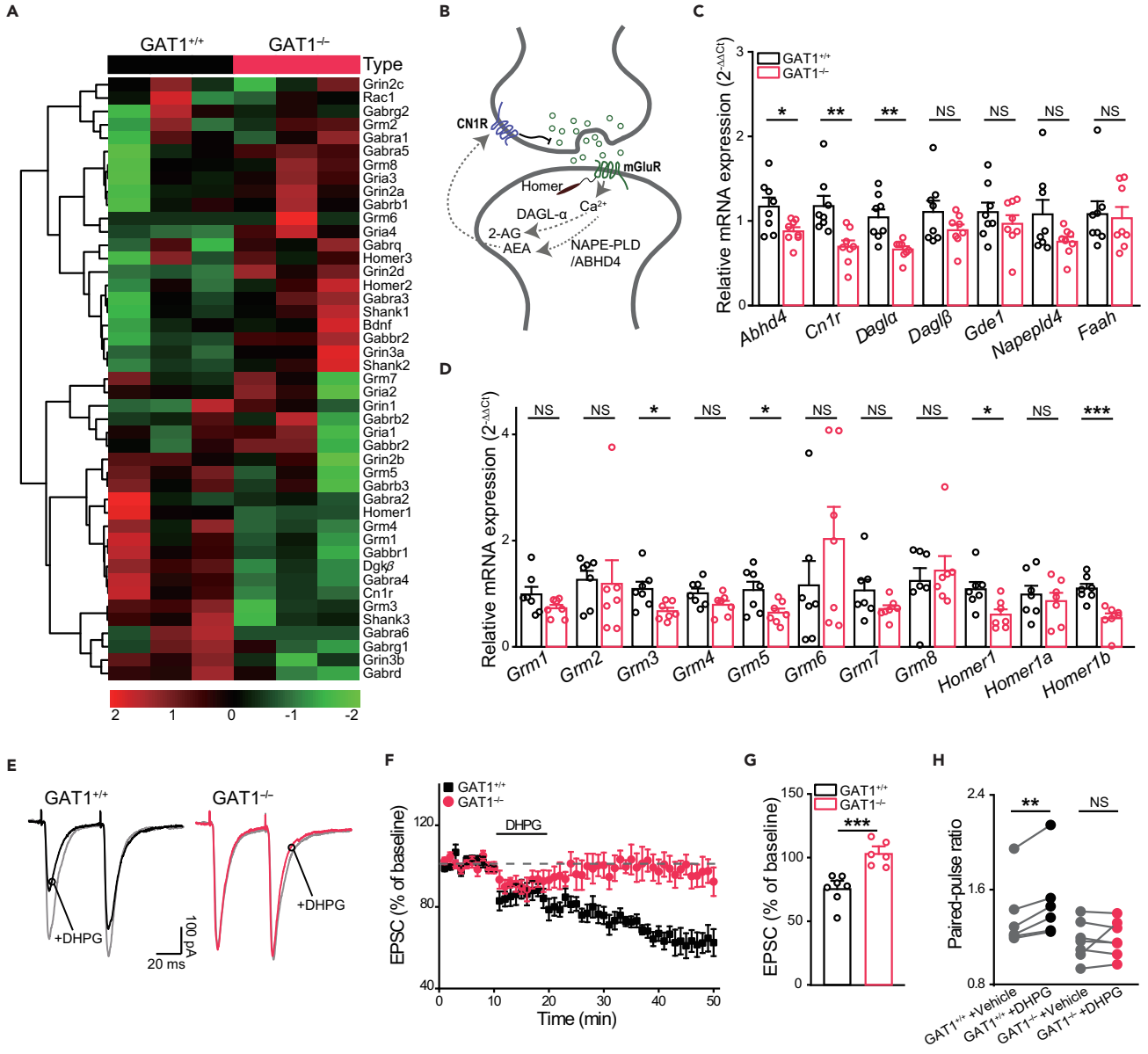


**Figure 4. Impaired mGluR-eCB signaling in the corticostriatal pathways of the GAT1$^{-/-}$ mice**

(A–D) Gene profile changes in the striatum of the GAT1$^{-/-}$ mice by RNA sequencing and RT-qPCR. (A) Heatmap of 45 genes in the striata of the GAT1$^{+/+}$ and GAT1$^{-/-}$ mice, based on FPKM (fragments per kilobase of transcript per million). (B) Schematic diagram for synaptic interactions of mGluRs and endocannabinoid signaling. (C and D) Verification of mRNA changes by qPCR. Data were normalized to GAPDH of the GAT1$^{+/+}$ group. Unpaired Student's *t* test, n = 7 to 8 mice for each group.

(E–H) DHPG-induced LTD at the corticostriatal pathways. (E) Representative traces of paired-pulse responses with 50-ms interval. (F) Time courses of DHPG-induced LTD in the corticostriatal synapses. Two-way repeated measures ANOVA, main effects of genotype, $F_{1,520} = 572.558$, $p < 0.001$, n = 7 neurons from five GAT1$^{+/+}$ mice and n = 6 neurons from four GAT1$^{-/-}$ mice. (G and H) Quantification of eEPSC changes based on the first peak at 30 min after the DHPG treatment compared to that at the baseline (G) and PPRs before and 30 min after the DHPG treatment (H). Unpaired Student's *t* test, n = 6 neurons from five GAT1$^{+/+}$ mice and n = 7 neurons from four GAT1$^{-/-}$ mice.

Data are represented as mean ± SEM. *, $p < 0.05$, **, $p < 0.01$, ***, $p < 0.001$, NS, no significant significance.

reduced (Figures 4C and 4D). Furthermore, the mRNA levels of the mGluR subunits, *Grm3* and *Grm5*, but not that of *Grm1*, *Grm2*, *Grm4*, *Grm6*, *Grm7*, or *Grm8*, were decreased in the striatum of the GAT1$^{-/-}$ mice, along with decreases in the mRNA levels of *Homer1* and *Homer1b*, but not that of *Homer1a* (Figure 4D). These results suggest that the mGluR-eCB signaling is disrupted in the striatum of the GAT1$^{-/-}$ mice.

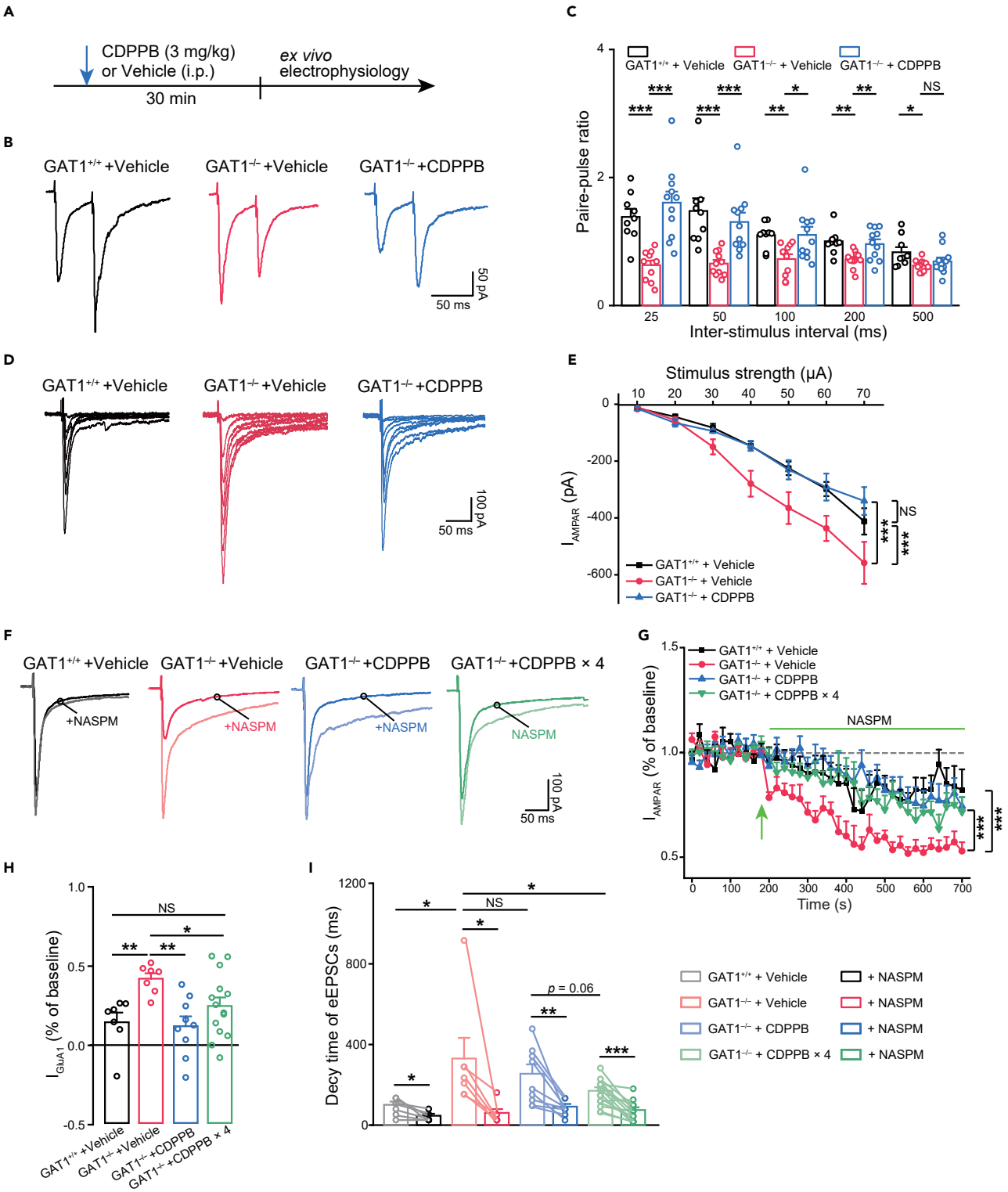


**Figure 5. Restoring mGluR activity reverses aberrant excitatory synaptic enhancement at the corticostriatal projections in the GAT1$^{-/-}$ mice**

(A) Experimental scheme.

(B and C) Effects of CDPPB on PPRs. Unpaired Student's *t* test, GAT1$^{+/+}$ + Vehicle group, n = 9 neurons from three mice; GAT1$^{-/-}$ + Vehicle group, n = 11 neurons from three mice; GAT1$^{-/-}$ + CDPPB group, n = 11 neurons from three mice.

**Figure 5. *Continued***

(D and E) Effects of CDPPB on AMPAR-mediated currents in the GAT1$^{-/-}$ mice. Two-way repeated measures ANOVA, main effects of CDPPB, $F_{2,156} = 17.519$, $p < 0.001$, GAT1$^{+/+}$ + Vehicle group, n = 10 neurons from three mice; GAT1$^{-/-}$ + Vehicle group, n = 11 neurons from three mice; GAT1$^{-/-}$ + CDPPB group, n = 9 neurons from three mice.

(F–I) Acute and chronic effects of *in vivo* CDPPB treatment on eEPSCs in the GAT1$^{-/-}$ mice. (F) Representative traces. (G) Amplitudes of eEPSCs before and after bath application of NASPM. Two-way repeated measures ANOVA, main effects of CDPPB, $F_{3,962} = 56.024$, $p < 0.001$. (H) Quantification of homomeric GluA1-mediated eEPSCs based on current at 5 min after NASPM application normalized to the baseline. One-way ANOVA, $F_{3,37} = 4.543$, $p = 0.009$. (I) Quantification of decay time of eEPSCs before and after NASPM application. Unpaired Student's *t* test and paired Student's *t* test, GAT1$^{+/+}$ + Vehicle group, n = 7 neurons from three mice; GAT1$^{-/-}$ + Vehicle group, n = 7 neurons from three mice; GAT1$^{-/-}$ + CDPPB group, n = 9 neurons from four mice; GAT1$^{-/-}$ + CDPPB × 4 group, n = 14 neurons from three mice.

Data are represented as mean ± SEM. *, $p < 0.05$, **, $p < 0.01$, ***, $p < 0.001$, NS, no significant significance.

## Impaired mGluR-eCB signaling in corticostriatal pathways of the GAT1$^{-/-}$ mice

The most prominent form of synaptic plasticity in the striatum is long-term depression (LTD), which involves the activation of mGluRs and a subsequent release of endocannabinoid.[58] During this process, eCBs like AEA and 2-AG are released by postsynaptic neurons and act as retrograde messengers to activate presynaptic CN1Rs, which in turn depress synaptic transmission.[61] To examine the effect of GAT1 disruption on mGluR-eCB signaling, we used 3,5-dihydroxyphenylglycine (DHPG, 50 μM, 10 min) to activate mGluRs. A paired electrical pulse stimulation with a 50-ms inter-stimulus interval was delivered before, during, and after the application of DHPG to assess the presynaptic function. DHPG induced LTD in almost all of the recorded MSNs from the GAT1$^{+/+}$ mice, with the first peak amplitude of eEPSC induced by paired electrical pulse stimulation decreased throughout the periods during and after the DHPG application (Figures 4E–4G). Notably, such a reduction of eEPSC amplitude did not occur in the GAT1$^{-/-}$ mice. Moreover, after the DHPG induction, PPRs increased in the GAT1$^{+/+}$ but not in the GAT1$^{-/-}$ mice (Figure 4H), implying that this plasticity is expressed presynaptically. Therefore, LTD via mGluR-eCB signaling in the corticostriatal pathways is disrupted in the GAT1$^{-/-}$ mice.

## Restoring mGluR-eCB signaling reverses aberrant excitatory synaptic enhancement in GAT1$^{-/-}$ mice

CDPPB, a positive allosteric modulator of mGluR5, is able to cross the brain-blood barrier and has been proposed to improve sensorimotor[62] and cognition[63,64] functions in rodent models. To establish a mechanistic link between the impaired mGluR-eCB signaling and homeostatic synaptic scaling up, we investigated whether activation of mGluR5 by CDPPB could rescue the corticostriatal synaptic abnormalities in the GAT1$^{-/-}$ mice. Whole-cell recordings were performed on acute brain slices prepared from GAT1$^{+/+}$ and GAT1$^{-/-}$ mice 2 h after i.p. injection of vehicle or CDPPB (Figure 5A). Consistent with the results shown in Figures 1K–1N, the vehicle-injected GAT1$^{-/-}$ mice showed decreased PPRs compared with the GAT1$^{+/+}$ mice. The injection of CDPPB in the GAT1$^{-/-}$ mice, however, reversed the PPRs to levels of the GAT1$^{+/+}$ mice, implying that the aberrant enhancement of presynaptic release probability in the GAT1$^{-/-}$ mice was completely corrected (Figures 5B and 5C). Furthermore, the increases in AMPAR-mediated eEPSC amplitude and in the proportion of CP-AMPAR-mediated eEPSCs were largely reversed by the CDPPB treatment at the corticostriatal pathways of the GAT1$^{-/-}$ mice (Figures 5D–5H). A single injection of CDPPB in the GAT1$^{-/-}$ mice was unable to reverse the prolonged decay time of eEPSCs to the level of GAT1$^{+/+}$ mice. However, in the GAT1$^{-/-}$ mice injected with CDPPB once daily for four consecutive days (CDPPB × 4), the eEPSC amplitude was reversed, while decaying more rapidly than in vehicle only mice (Figures 5F and 5I). NASPM reduced the decay time of eEPSCs in brain slices of GAT1$^{+/+}$ and GAT1$^{-/-}$ mice, with or without CDPPB treatment (Figure 5I), implying that CP-AMPAR dynamics may underlie the potential therapeutic effect of CDPPB. These results suggest that homeostatic synaptic scaling in the GAT1$^{-/-}$ mice depends on the downregulation of mGluR-eCB signaling at the corticostriatal projections.

## Pharmacological potentiation of mGluR-eCB signaling or blockade of homomeric-GluA1 reverses locomotor hyperactivity in the GAT1$^{-/-}$ mice

To test whether the impaired mGluR-eCB signaling in GAT1$^{-/-}$ mice is responsible for the locomotor hyperactivity, we injected the agonist of CN1R or mGluRs, WIN 55,212-2 (WIN) and CDPPB, respectively, into the mice before the open-field test (Figure 6A). Notably, the GAT1$^{-/-}$ mice injected with WIN or CDPPB showed a significant improvement in locomotor activity, to levels comparable to that of the GAT1$^{+/+}$ mice (Figures 6B and 6C). Because the impaired mGluR-eCB signaling mediates the scaling up of CP-AMPARs, we investigated whether such an enhanced excitatory synaptic drive at the corticostriatal synapses was responsible for locomotor hyperactivity in GAT1$^{-/-}$ mice. NASPM, but vehicle, injected bilaterally into

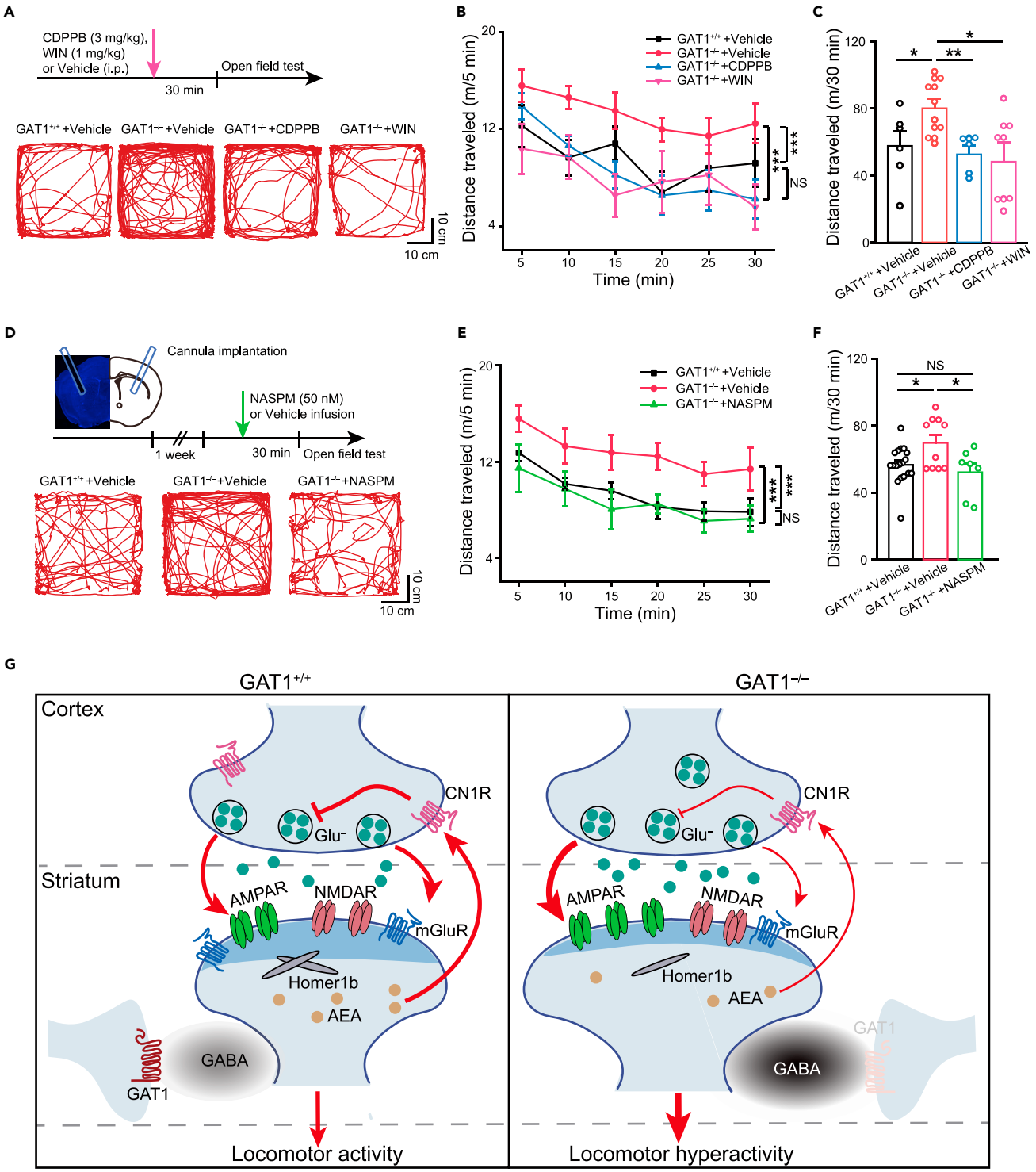


**Figure 6. Both potentiation of mGluR-eCB signaling and inhibition of GluA1 reverse locomotor hyperactivity of the GAT1$^{-/-}$ mice**

(A–C) Effect of potentiation of mGluR-eCB signaling on locomotor hyperactivity of the GAT1$^{-/-}$ mice. (A) Experimental scheme and representative traces of distance traveled during the first 5 min in the open field test. (B) Distance traveled in individual 5-min intervals within the 30-min test. Two way repeated-measures ANOVA, main effects of drugs, $F_{3,150} = 14.06$, $p < 0.001$. (C) Total distance traveled during the entire 30-min test. One-way ANOVA, $F_{3,26} = 4.294$, $p = 0.016$, GAT1$^{+/+}$ + Vehicle group, n = 6 mice; GAT1$^{-/-}$ + Vehicle group, n = 9 mice; GAT1$^{-/-}$ + CDPPB group, n = 5 mice; GAT1$^{-/-}$ + WIN group, n = 6 mice. (D–F) Effects of inhibition of GluA1 in striatum on locomotor hyperactivity of the GAT1$^{-/-}$ mice. (D) Schematics of cannula implantation, experimental scheme and representative traces of distance traveled during the first 5 min in the open field test. (E) Distance traveled in individual 5-min intervals within the

**Figure 6. *Continued***

30-min test. Two-way repeated measures ANOVA, main effects of NASPM, $F_{2,180} = 18.871$, $p < 0.001$. (F) Total distance traveled during the entire 30-min test. One-way ANOVA, $F_{2,30} = 4.310$, $p = 0.024$, $GAT1^{+/+}$ + Vehicle group, n = 15 mice; $GAT1^{-/-}$ + Vehicle group, n = 8 mice; $GAT1^{-/-}$ + NASPM group, n = 7 mice.

(G) Schematic diagrams of synaptic scaling of the corticostriatal circuits, which underlies hyperactivity caused by GAT1 deficiency. In the $GAT1^{-/-}$ mice, downregulation of mGluR-eCB signaling at the corticostriatal projections underlies scaling up of excitatory synaptic transmission, which confers schizophrenia-associated locomotor hyperactivity.

Data are represented as mean ± SEM. *, $p < 0.05$, **, $p < 0.01$, ***, $p < 0.001$, NS, no significant significance.

the dorsal striatum 30 min before the open field test, significantly reversed the locomotor hyperactivity of the $GAT1^{-/-}$ mice (Figures 6D–6F). Altogether, our results establish the notion that in adolescent $GAT1^{-/-}$ mice, downregulation of mGluR-eCB signaling at the corticostriatal projections underlies the scaling up of excitatory synaptic transmission, which confers schizophrenia-associated locomotor hyperactivity (Figure 6G). These data reveal a previously unknown role of synaptic scaling in the corticostriatal pathways to locomotor hyperactivity, to which counteracting represents a potential therapeutic strategy.

## DISCUSSION

Although homeostatic synaptic scaling helps maintain a steady-state of the central nervous system by restoring neural network activity from perturbation, it also complicates the etiological mechanisms of neuropsychiatry disorders with E-I imbalance, including schizophrenia. In the current study, using adolescent mice with GAT1 gene ablation and prolonged drug inhibition of GAT1 from weaning in the wild type background, which both displayed a behavioral phenotype of locomotor hyperactivity, we identified an excitatory synaptic scaling in the corticostriatal pathways in response to GAT1 disruption. Genetic deletion of GAT1 led to an increased percentage of mature dendritic spines and an increased proportion of homomeric-GluA1 AMPARs at the corticostriatal excitatory synapses. Striatum-specific pharmacological inhibition of the homomeric-GluA1 AMPARs rescued locomotor hyperactivity in the $GAT1^{-/-}$ mice, suggesting that scaling up of the corticostriatal synapses was sufficient to confer such type of schizophrenia-related locomotor hyperactivity. To investigate the underlying mechanisms, we identified an inactivation of mGluR-eCB signaling which largely mediated the corticostriatal synaptic scaling caused by GAT1 disruption. Furthermore, pharmacological restoration of the mGluR-eCB signaling reversed the aberrant excitatory synaptic enhancement and ameliorated locomotor hyperactivity in the $GAT1^{-/-}$ mice. Our data reveal a significant role of synaptic scaling in the corticostriatal pathways to locomotor hyperactivity associated with schizophrenia (Figure 6G), thus providing alternative targets for potential therapeutic strategies.

Increasing studies support that homeostatic synaptic remodeling plays a key role not only in activity-dependent neurodevelopment but also in the pathogenesis of a variety of neurodevelopmental disorders. During the critical period of development, scaling up or down of global synaptic inputs is critically engaged in sensory activity-dependent refinement of cortical connectivity. Deprivation of visual inputs during early postnatal days significantly enhances spontaneous neuronal activity in the visual cortex in a layer- and age-dependent manner through a set of homeostatic plasticity mechanisms,[65–71] including increased net excitatory and decreased net inhibitory synaptic drive. Coincidentally, the Rett syndrome protein methyl-CpG binding protein 2 (MeCP2) plays a crucial role in both homeostatic synaptic scaling down[72,73] and scaling up,[74] in response to increased and decreased neuronal firing, respectively. Notably, a mouse model of Rett syndrome with MeCP2 deletion prevents homeostatic synaptic scaling up to visual deprivation *in vivo*.[74] These results provoke an interesting possibility that the pathophysiology of Rett syndrome, which is caused by mutations of MeCP2, may arise from a disruption of homeostatic plasticity. Meanwhile, the autism-associated Shank3 protein is indispensable for homeostatic compensation in visual cortical circuits.[75] A reduction of homeostatic responses has been demonstrated in brain slices or cultured neurons from mice with mutations in autism-associated genes, fragile X mental retardation protein (FMRP),[76,77] and chromodomain helicase DNA binding protein 8 (CHD8).[78] In contrast to the above examples of neurodevelopmental disorders caused by the failure to compensate for neural network perturbance, we demonstrate that the deficiency of GABA recycling results in a maladaptive scaling up at the corticostriatal synapses, eventually leading to locomotor hyperactivity, a behavioral phenotype associated with schizophrenia. It is worth pointing out that unlike the above disease models, the $GAT1^{-/-}$ mice used in the current study maintain the complete molecular machinery of homeostatic synaptic remodeling. Our finding thus complements the view that both insufficient and maladaptive homeostatic mechanisms take effect on multiple facets of neurodevelopmental disorders.

In contrast to the intensively studied synaptic scaling mechanisms in cortical and hippocampal neurons,[8] molecular mechanisms underlying homeostatic scaling of the corticostriatal synapses remain largely unexplored. Homeostatic synaptic plasticity in the striatum involves several signaling elements that ultimately drive activity-dependent changes in synaptic function. In aged BACHD mice, a slowly progressive Huntington's disease model, the loss of dendritic spines in MSNs serves as an initial perturbing factor that increases the strength of the remaining synapses and intrinsic neuronal activity to compensate for the spine shortfall.[79] Mechanistically, the spine loss in the striatum is accompanied by a downregulation of the striatum-specific G protein-coupled receptor 88 (Gpr88) and a high GluA1/GluA2 ratio. In our adolescent mouse model of the GAT1$^{-/-}$ mice, we found a decrease in spine density in the MSNs but an increase in the proportion of mature dendritic spines, an increase in the expression of GluA1 but not GluA2 subunits, and therefore a high GluA1/GluA2 ratio and an increase in the proportion of CP-AMPARs at the corticostriatal excitatory synapses. Notably, pharmacological inhibition of CP-AMPARs at the striatum corrected locomotor hyperactivity of the GAT1$^{-/-}$ mice, suggesting that an aberrant gain-of-function of the corticostriatal synapses mediated these schizophrenia-related behavioral symptoms. We further identified a reduction in mGluR-eCB signaling in the GAT1$^{-/-}$ mice that mediated homeostatic scaling up at the corticostriatal synapses. These findings are reminiscent of a previous study that reductions in endocannabinoid tone served as a homeostatic mechanism for specific inhibitory synapses in hippocampal networks,[80] suggesting that at least some shared signaling pathways constitute the negative feedback system under the control of network activity. Of interest, our RNA-Seq results demonstrated that the transcript of *Gpr88* in adolescent GAT1$^{-/-}$ mice was reduced compared to the GAT1$^{+/+}$ mice (data not shown), as was also the case in aged BACHD mice,[79] implying that *Gpr88* may be involved in the striatal synaptic scaling under different pathological scenarios.

In the striatum, mGluRs modulate synaptic transmission by affecting cellular excitability, ionic conductance, and neurotransmitter release.[57] Activation of group I mGluRs generates eCBs, which act as retrograde messengers to activate presynaptic CN1R, thereby depressing synaptic transmission.[61] This way of postsynaptic induction to dampen presynaptic actions employed by mGluR-LTD entails an ideal synaptic scaling mechanism in response to synaptic input perturbation, which has been implicated in striatum-related neurological diseases.[56,81] In the current study, we added the schizophrenia-related locomotor hyperactivity to the list of pathophysiological significance of the striatal mGluR-LTD, which provides novel insights into understanding the mechanisms underlying mGluRs as emerging targets for the treatment of schizophrenia.[82] Nevertheless, the precise cellular and molecular mechanisms underlying the inactivation of such plasticity in response to GAT1 disruption remain elusive and need to be clarified in future studies. At the synapse, mGluRs are anchored by Homer proteins in a complex that clusters together ionotropic and metabotropic glutamate receptors.[83] Meanwhile, altered mGluR5-Homer scaffolds play a major contribution to the phenotype and synaptic deficits in the *Fmr1* knockout (KO) mice.[84] Notably, in the corticostriatal pathways of the adolescent GAT1$^{-/-}$ mice, we found the expression of Homer1 and Homer1b, but not Homer1a, to be downregulated in parallel with that of mGluR5, suggesting the GAT1-regulated mGluR5-Homer1b signaling for striatal synapse function. Previous studies have shown that in postmortem schizophrenia cohorts, mRNA and protein levels of Homer1b/c and group I mGluRs are concomitantly altered in the hippocampus and cortex,[85,86] supporting that a general coupling between mGluR5 and Homer1b is associated with schizophrenia.

In conclusion, our study reveals that in the striatum of GAT1-deficient mice, where GABA recycling is impaired, scaling up of the corticostriatal excitatory synapses underlies the locomotor hyperactivity, a phenotype associated with schizophrenia. Furthermore, our findings suggest that inactivation of mGluR-eCB signaling and resultant LTD serves as the homeostatic mechanism of the maladaptive scaling in the GAT1-deficient mice, and correspondingly antagonizing either CP-AMPARs, or mGluRs or CN1R - the main consequences or drives of synaptic scaling up, respectively - reverses these behavioral deficits. This study represents a significant advancement in the crucial involvement of compensatory enhancement of the corticostriatal excitatory synapse on a net increase of GABAergic inhibition in schizophrenia-locomotor hyperactivity and provides new insights into the cellular mechanisms of locomotor hyperactive psychotic symptoms. These findings can inform novel therapeutic approaches for the treatment of such devastating neurodevelopmental disorders.

## Limitations of the study

The molecular mechanisms of elimination of DHPG-induced LTD in GAT1$^{-/-}$ were still not fully understood yet. In addition to the reduced mRNA levels for mGluR5 but not mGluR1, the protein levels and the resulting

functions of these mGluRs should be examined more carefully in future studies. Moreover, along with decreases in the mRNA levels of the mGluR subunits in the striatum of the GAT1$^{-/-}$ mice, mRNA levels of Homer1 and Homer1b were also downregulated, suggesting the GAT1-regulated mGluR5-Homer1b signaling was important for striatal synapse function, although the exact molecular cascade remained unclear. Finally, molecular underpinnings of different adaptations of AMPARs and mGluRs in the striatum of the GAT1$^{-/-}$ mice remained to be established. In the current study, these two kinds of glutamate receptors were up- and down-regulated in the GAT1$^{-/-}$ mice, respectively, compared to wild type mice. In this issue, the same pool of glutamate released from cortical neurons would result in enhanced or reduced AMPAR and mGluR function, respectively. The detail mechanisms remained to be determined in the future studies.

## STAR★METHODS

Detailed methods are provided in the online version of this paper and include the following:

- KEY RESOURCES TABLE
- RESOURCE AVAILABILITY
  - Lead contact
  - Materials availability
  - Data and code availability
- EXPERIMENTAL MODEL AND SUBJECT DETAILS
  - Mice
- METHOD DETAILS
  - Brain slice electrophysiology
  - Western blotting
  - Electron microscopy (EM) and Golgi-Cox staining
  - Surgical procedures and drug delivery
  - Open field test
  - RNA sequencing
  - Quantitative real-time PCR
  - Liquid chromatograph mass spectrometer
- QUANTIFICATION AND STATISTICAL ANALYSIS

## SUPPLEMENTAL INFORMATION

Supplemental information can be found online at https://doi.org/10.1016/j.isci.2023.106322.

## ACKNOWLEDGMENTS

We thank Dr. Jian Fei from Shanghai Model Organisms Center for kindly providing the GAT1$^{-/-}$ mice used in the current study. We thank Drs. Zhe Yu, Neng Gong, and Nan-Jie Xu for fruitful discussion. We thank Ze-Jie Lin and Zhi-Han Jiao for technical support. This study was supported by grants from the STI2030-Major Projects (2021ZD0202802), the National Natural Science Foundation of China (31930050, 32071023, 31900701, 81903583, and 81771214), the Shanghai Municipal Science and Technology Major Project (2018SHZDZX05), the Science and Technology Commission of Shanghai Municipality (22XD1420700), the Shanghai Municipal Health Commission (2022XD046), and innovative research team of high-level local universities in Shanghai. Dr. Yan-Jiao Wu is awarded the fellowship of China Postdoctoral Science Foundation (2021T140456).

## AUTHOR CONTRIBUTIONS

Conceptualization, Y-J.W., W.-G.L., and T-L.X.; Methodology, Y-J.W. and X.Y.; Investigation, Y-J.W., X.Y., X.G., Q.W., Q.J., and Y.L.; Writing – Original Draft, Y-J.W., W.-G.L., and T-L.X.; Writing – Review and Editing, Y-J.W., M-X.Z., W-G.L., and T-L.X.; Funding Acquisition, Y-J.W., J.D., W-G.L., and T-L.X.; Resources, Y-J.W., J.D., W-G.L., and T-L.X.; Supervision, J.D., W-G.L., and T-L.X.

## DECLARATION OF INTERESTS

The authors declare no competing interests.

## INCLUSION AND DIVERSITY

We support inclusive, diverse, and equitable conduct of research.

Received: July 13, 2022
Revised: September 21, 2022
Accepted: February 27, 2023
Published: March 3, 2023

## REFERENCES

1. Davis, G.W. (2006). Homeostatic control of neural activity: from phenomenology to molecular design. Annu. Rev. Neurosci. *29*, 307–323. https://doi.org/10.1146/annurev.neuro.28.061604.135751.

2. Pozo, K., and Goda, Y. (2010). Unraveling mechanisms of homeostatic synaptic plasticity. Neuron *66*, 337–351. https://doi.org/10.1016/j.neuron.2010.04.028.

3. Tang, X., Jaenisch, R., and Sur, M. (2021). The role of GABAergic signalling in neurodevelopmental disorders. Nat. Rev. Neurosci. *22*, 290–307. https://doi.org/10.1038/s41583-021-00443-x.

4. Rao, A., and Craig, A.M. (1997). Activity regulates the synaptic localization of the NMDA receptor in hippocampal neurons. Neuron *19*, 801–812. https://doi.org/10.1016/s0896-6273(00)80962-9.

5. O'Brien, R.J., Kamboj, S., Ehlers, M.D., Rosen, K.R., Fischbach, G.D., and Huganir, R.L. (1998). Activity-dependent modulation of synaptic AMPA receptor accumulation. Neuron *21*, 1067–1078. https://doi.org/10.1016/s0896-6273(00)80624-8.

6. Turrigiano, G.G., Leslie, K.R., Desai, N.S., Rutherford, L.C., and Nelson, S.B. (1998). Activity-dependent scaling of quantal amplitude in neocortical neurons. Nature *391*, 892–896. https://doi.org/10.1038/36103.

7. Murthy, V.N., Schikorski, T., Stevens, C.F., and Zhu, Y. (2001). Inactivity produces increases in neurotransmitter release and synapse size. Neuron *32*, 673–682. https://doi.org/10.1016/s0896-6273(01)00500-1.

8. Turrigiano, G.G. (2008). The self-tuning neuron: synaptic scaling of excitatory synapses. Cell *135*, 422–435. https://doi.org/10.1016/j.cell.2008.10.008.

9. Kleinjan, M.S., Buchta, W.C., Ogelman, R., Hwang, I.W., Kuwajima, M., Hubbard, D.D., Kareemo, D.J., Prikhodko, O., Olah, S.L., Gomez Wulschner, L.E., et al. (2023). Dually innervated dendritic spines develop in the absence of excitatory activity and resist plasticity through tonic inhibitory crosstalk. Neuron *111*, 362–371.e6. https://doi.org/10.1016/j.neuron.2022.11.002.

10. Colameo, D., and Schratt, G. (2022). Synaptic tagging: homeostatic plasticity goes Hebbian. EMBO J. *41*, e112383. https://doi.org/10.15252/embj.2022112383.

11. Diering, G.H., Nirujogi, R.S., Roth, R.H., Worley, P.F., Pandey, A., and Huganir, R.L. (2017). Homer1a drives homeostatic scaling-down of excitatory synapses during sleep. Science *355*, 511–515. https://doi.org/10.1126/science.aai8355.

12. Wu, C.H., Ramos, R., Katz, D.B., and Turrigiano, G.G. (2021). Homeostatic synaptic scaling establishes the specificity of an associative memory. Curr. Biol. *31*, 2274–2285.e5. https://doi.org/10.1016/j.cub.2021.03.024.

13. Turrigiano, G.G., and Nelson, S.B. (2004). Homeostatic plasticity in the developing nervous system. Nat. Rev. Neurosci. *5*, 97–107. https://doi.org/10.1038/nrn1327.

14. Turrigiano, G. (2011). Too many cooks? Intrinsic and synaptic homeostatic mechanisms in cortical circuit refinement. Annu. Rev. Neurosci. *34*, 89–103. https://doi.org/10.1146/annurev-neuro-060909-153238.

15. Froemke, R.C. (2015). Plasticity of cortical excitatory-inhibitory balance. Annu. Rev. Neurosci. *38*, 195–219. https://doi.org/10.1146/annurev-neuro-071714-034002.

16. Nelson, S.B., and Valakh, V. (2015). Excitatory/inhibitory balance and circuit homeostasis in autism spectrum disorders. Neuron *87*, 684–698. https://doi.org/10.1016/j.neuron.2015.07.033.

17. Antoine, M.W., Langberg, T., Schnepel, P., and Feldman, D.E. (2019). Increased excitation-inhibition ratio stabilizes synapse and circuit excitability in four autism mouse models. Neuron *101*, 648–661.e4. https://doi.org/10.1016/j.neuron.2018.12.026.

18. Deidda, G., Bozarth, I.F., and Cancedda, L. (2014). Modulation of GABAergic transmission in development and neurodevelopmental disorders: investigating physiology and pathology to gain therapeutic perspectives. Front. Cell. Neurosci. *8*, 119. https://doi.org/10.3389/fncel.2014.00119.

19. Schmidt, M.J., and Mirnics, K. (2015). Neurodevelopment, GABA system dysfunction, and schizophrenia. Neuropsychopharmacology *40*, 190–206. https://doi.org/10.1038/npp.2014.95.

20. Guastella, J., Nelson, N., Nelson, H., Czyzyk, L., Keynan, S., Miedel, M.C., Davidson, N., Lester, H.A., and Kanner, B.I. (1990). Cloning and expression of a rat brain GABA transporter. Science *249*, 1303–1306. https://doi.org/10.1126/science.1975955.

21. Durkin, M.M., Smith, K.E., Borden, L.A., Weinshank, R.L., Branchek, T.A., and Gustafson, E.L. (1995). Localization of messenger RNAs encoding three GABA transporters in rat brain: an in situ hybridization study. Brain Res. Mol. Brain Res. *33*, 7–21. https://doi.org/10.1016/0169-328x(95)00101-w.

22. Yasumi, M., Sato, K., Shimada, S., Nishimura, M., and Tohyama, M. (1997). Regional distribution of GABA transporter 1 (GAT1) mRNA in the rat brain: comparison with glutamic acid decarboxylase67 (GAD67) mRNA localization. Brain Res. Mol. Brain Res. *44*, 205–218. https://doi.org/10.1016/s0169-328x(96)00200-8.

23. Lewis, D.A., and Gonzalez-Burgos, G. (2006). Pathophysiologically based treatment interventions in schizophrenia. Nat. Med. *12*, 1016–1022. https://doi.org/10.1038/nm1478.

24. Rees, E., Han, J., Morgan, J., Carrera, N., Escott-Price, V., Pocklington, A.J., Duffield, M., Hall, L.S., Legge, S.E., Pardiñas, A.F., et al. (2020). De novo mutations identified by exome sequencing implicate rare missense variants in SLC6A1 in schizophrenia. Nat. Neurosci. *23*, 179–184. https://doi.org/10.1038/s41593-019-0565-2.

25. Carvill, G.L., McMahon, J.M., Schneider, A., Zemel, M., Myers, C.T., Saykally, J., Nguyen, J., Robbiano, A., Zara, F., Specchio, N., et al. (2015). Mutations in the GABA transporter SLC6A1 cause epilepsy with myoclonic-atonic seizures. Am. J. Hum. Genet. *96*, 808–815. https://doi.org/10.1016/j.ajhg.2015.02.016.

26. Mattison, K.A., Butler, K.M., Inglis, G.A.S., Dayan, O., Boussidan, H., Bhambhani, V., Philbrook, B., da Silva, C., Alexander, J.J., Kanner, B.I., and Escayg, A. (2018). SLC6A1 variants identified in epilepsy patients reduce gamma-aminobutyric acid transport. Epilepsia *59*, e135–e141. https://doi.org/10.1111/epi.14531.

27. Kahen, A., Kavus, H., Geltzeiler, A., Kentros, C., Taylor, C., Brooks, E., Green Snyder, L., and Chung, W. (2022). Neurodevelopmental phenotypes associated with pathogenic variants in SLC6A1. J. Med. Genet. *59*, 536–543. https://doi.org/10.1136/jmedgenet-2021-107694.

28. Mermer, F., Poliquin, S., Rigsby, K., Rastogi, A., Shen, W., Romero-Morales, A., Nwosu, G., McGrath, P., Demerast, S., Aoto, J., et al. (2021). Common molecular mechanisms of SLC6A1 variant-mediated neurodevelopmental disorders in astrocytes and neurons. Brain *144*, 2499–2512. https://doi.org/10.1093/brain/awab207.

29. Poliquin, S., Hughes, I., Shen, W., Mermer, F., Wang, J., Mack, T., Xu, D., and Kang, J.Q. (2021). Genetic mosaicism, intrafamilial phenotypic heterogeneity, and molecular defects of a novel missense SLC6A1 mutation associated with epilepsy and ADHD. Exp. Neurol. *342*, 113723. https://doi.org/10.1016/j.expneurol.2021.113723.

30. Gong, N., Li, Y., Cai, G.Q., Niu, R.F., Fang, Q., Wu, K., Chen, Z., Lin, L.N., Xu, L., Fei, J., and Xu, T.L. (2009). GABA transporter-1 activity modulates hippocampal theta oscillation and theta burst stimulation-induced long-term potentiation. J. Neurosci. *29*, 15836–15845. https://doi.org/10.1523/JNEUROSCI.4643-09.2009.

31. Yu, Z., Fang, Q., Xiao, X., Wang, Y.Z., Cai, Y.Q., Cao, H., Hu, G., Chen, Z., Fei, J., Gong, N., and Xu, T.L. (2013). GABA transporter-1 deficiency confers schizophrenia-like behavioral phenotypes. PLoS One *8*, e69883. https://doi.org/10.1371/journal.pone.0069883.

32. Forrest, A.D., Coto, C.A., and Siegel, S.J. (2014). Animal models of psychosis: current state and future directions. Curr. Behav. Neurosci. Rep. *1*, 100–116. https://doi.org/10.1007/s40473-014-0013-2.

33. Simpson, E.H., Kellendonk, C., and Kandel, E. (2010). A possible role for the striatum in the pathogenesis of the cognitive symptoms of schizophrenia. Neuron *65*, 585–596. https://doi.org/10.1016/j.neuron.2010.02.014.

34. Fornito, A., Harrison, B.J., Goodby, E., Dean, A., Ooi, C., Nathan, P.J., Lennox, B.R., Jones, P.B., Suckling, J., and Bullmore, E.T. (2013). Functional dysconnectivity of corticostriatal circuitry as a risk phenotype for psychosis. JAMA Psychiatr. *70*, 1143–1151. https://doi.org/10.1001/jamapsychiatry.2013.1976.

35. McCutcheon, R.A., Abi-Dargham, A., and Howes, O.D. (2019). Schizophrenia, dopamine and the striatum: from biology to symptoms. Trends Neurosci. *42*, 205–220. https://doi.org/10.1016/j.tins.2018.12.004.

36. Vyas, N.S., Kumra, S., and Puri, B.K. (2010). What insights can we gain from studying early-onset schizophrenia? The neurodevelopmental pathway and beyond. Expert Rev. Neurother. *10*, 1243–1247. https://doi.org/10.1586/ern.10.109.

37. Laviola, G., Macrì, S., Morley-Fletcher, S., and Adriani, W. (2003). Risk-taking behavior in adolescent mice: psychobiological determinants and early epigenetic influence. Neurosci. Biobehav. Rev. *27*, 19–31. https://doi.org/10.1016/s0149-7634(03)00006-x.

38. Augood, S.J., Herbison, A.E., and Emson, P.C. (1995). Localization of GAT-1 GABA transporter mRNA in rat striatum: cellular coexpression with GAD67 mRNA, GAD67 immunoreactivity, and parvalbumin mRNA. J. Neurosci. *15*, 865–874.

39. Ng, C.H., Wang, X.S., and Ong, W.Y. (2000). A light and electron microscopic study of the GABA transporter GAT-3 in the monkey basal ganglia and brainstem. J. Neurocytol. *29*, 595–603. https://doi.org/10.1023/a:1011076219493.

40. Jin, X.T., Galvan, A., Wichmann, T., and Smith, Y. (2011). Localization and function of GABA transporters GAT-1 and GAT-3 in the basal ganglia. Front. Syst. Neurosci. *5*, 63. https://doi.org/10.3389/fnsys.2011.00063.

41. Gunaydin, L.A., and Kreitzer, A.C. (2016). Cortico-basal ganglia circuit function in psychiatric disease. Annu. Rev. Physiol. *78*, 327–350. https://doi.org/10.1146/annurev-physiol-021115-105355.

42. Kreitzer, A.C. (2009). Physiology and pharmacology of striatal neurons. Annu. Rev. Neurosci. *32*, 127–147. https://doi.org/10.1146/annurev.neuro.051508.135422.

43. Kirmse, K., Kirischuk, S., and Grantyn, R. (2009). Role of GABA transporter 3 in GABAergic synaptic transmission at striatal output neurons. Synapse *63*, 921–929. https://doi.org/10.1002/syn.20675.

44. Zucker, R.S., and Regehr, W.G. (2002). Short-term synaptic plasticity. Annu. Rev. Physiol. *64*, 355–405. https://doi.org/10.1146/annurev.physiol.64.092501.114547.

45. Suzdak, P.D., Frederiksen, K., Andersen, K.E., Sørensen, P.O., Knutsen, L.J., and Nielsen, E.B. (1992). NNC-711, a novel potent and selective gamma-aminobutyric acid uptake inhibitor: pharmacological characterization. Eur. J. Pharmacol. *224*, 189–198. https://doi.org/10.1016/0014-2999(92)90804-d.

46. Harris, K.M., and Kater, S.B. (1994). Dendritic spines: cellular specializations imparting both stability and flexibility to synaptic function. Annu. Rev. Neurosci. *17*, 341–371. https://doi.org/10.1146/annurev.ne.17.030194.002013.

47. Sala, C., and Segal, M. (2014). Dendritic spines: the locus of structural and functional plasticity. Physiol. Rev. *94*, 141–188. https://doi.org/10.1152/physrev.00012.2013.

48. Sheng, M., and Hoogenraad, C.C. (2007). The postsynaptic architecture of excitatory synapses: a more quantitative view. Annu. Rev. Biochem. *76*, 823–847. https://doi.org/10.1146/annurev.biochem.76.060805.160029.

49. Henley, J.M., and Wilkinson, K.A. (2016). Synaptic AMPA receptor composition in development, plasticity and disease. Nat. Rev. Neurosci. *17*, 337–350. https://doi.org/10.1038/nrn.2016.37.

50. Ogoshi, F., Yin, H.Z., Kuppumbatti, Y., Song, B., Amindari, S., and Weiss, J.H. (2005). Tumor necrosis-factor-alpha (TNF-alpha) induces rapid insertion of Ca2+-permeable alpha-amino-3-hydroxyl-5-methyl-4-isoxazole-propionate (AMPA)/kainate (Ca-A/K) channels in a subset of hippocampal pyramidal neurons. Exp. Neurol. *193*, 384–393. https://doi.org/10.1016/j.expneurol.2004.12.026.

51. Thiagarajan, T.C., Lindskog, M., and Tsien, R.W. (2005). Adaptation to synaptic inactivity in hippocampal neurons. Neuron *47*, 725–737. https://doi.org/10.1016/j.neuron.2005.06.037.

52. Shepherd, J.D., Rumbaugh, G., Wu, J., Chowdhury, S., Plath, N., Kuhl, D., Huganir, R.L., and Worley, P.F. (2006). Arc/Arg3.1 mediates homeostatic synaptic scaling of AMPA receptors. Neuron *52*, 475–484. https://doi.org/10.1016/j.neuron.2006.08.034.

53. Sutton, M.A., Ito, H.T., Cressy, P., Kempf, C., Woo, J.C., and Schuman, E.M. (2006). Miniature neurotransmission stabilizes synaptic function via tonic suppression of local dendritic protein synthesis. Cell *125*, 785–799. https://doi.org/10.1016/j.cell.2006.03.040.

54. Aoto, J., Nam, C.I., Poon, M.M., Ting, P., and Chen, L. (2008). Synaptic signaling by all-trans retinoic acid in homeostatic synaptic plasticity. Neuron *60*, 308–320. https://doi.org/10.1016/j.neuron.2008.08.012.

55. Stincic, T.L., and Frerking, M.E. (2015). Different AMPA receptor subtypes mediate the distinct kinetic components of a biphasic EPSC in hippocampal interneurons. Front. Synaptic Neurosci. *7*, 7. https://doi.org/10.3389/fnsyn.2015.00007.

56. Gubellini, P., Pisani, A., Centonze, D., Bernardi, G., and Calabresi, P. (2004). Metabotropic glutamate receptors and striatal synaptic plasticity: implications for neurological diseases. Prog. Neurobiol. *74*, 271–300. https://doi.org/10.1016/j.pneurobio.2004.09.005.

57. Bonsi, P., Platania, P., Martella, G., Madeo, G., Vita, D., Tassone, A., Bernardi, G., and Pisani, A. (2008). Distinct roles of group I mGlu receptors in striatal function. Neuropharmacology *55*, 392–395. https://doi.org/10.1016/j.neuropharm.2008.05.020.

58. Kreitzer, A.C., and Malenka, R.C. (2008). Striatal plasticity and basal ganglia circuit function. Neuron *60*, 543–554. https://doi.org/10.1016/j.neuron.2008.11.005.

59. Lovinger, D.M. (2010). Neurotransmitter roles in synaptic modulation, plasticity and learning in the dorsal striatum. Neuropharmacology *58*, 951–961. https://doi.org/10.1016/j.neuropharm.2010.01.008.

60. Wu, Y.W., Kim, J.I., Tawfik, V.L., Lalchandani, R.R., Scherrer, G., and Ding, J.B. (2015). Input- and cell-type-specific endocannabinoid-dependent LTD in the striatum. Cell Rep. *10*, 75–87. https://doi.org/10.1016/j.celrep.2014.12.005.

61. Kano, M., Ohno-Shosaku, T., Hashimotodani, Y., Uchigashima, M., and Watanabe, M. (2009). Endocannabinoid-mediated control of synaptic transmission. Physiol. Rev. *89*, 309–380. https://doi.org/10.1152/physrev.00019.2008.

62. Brown, R.W., Varnum, C.G., Wills, L.J., Peeters, L.D., and Gass, J.T. (2021). Modulation of mGlu5 improves sensorimotor gating deficits in rats neonatally treated with quinpirole through changes in dopamine D2 signaling. Pharmacol. Biochem. Behav. *211*, 173292. https://doi.org/10.1016/j.pbb.2021.173292.

63. Bellozi, P.M.Q., Gomes, G.F., da Silva, M.C.M., Lima, I.V.d.A., Batista, C.R.Á., Carneiro Junior, W.d.O., Dória, J.G., Vieira, É.L.M., Vieira, R.P., de Freitas, R.P., et al.

(2019). A positive allosteric modulator of mGluR5 promotes neuroprotective effects in mouse models of Alzheimer's disease. Neuropharmacology *160*, 107785. https://doi.org/10.1016/j.neuropharm.2019.107785.

64. Płoska, A., Cieślik, P., Siekierzycka, A., Kalinowski, L., and Wierońska, J.M. (2021). Neurochemical changes underlying cognitive impairment in olfactory bulbectomized rats and the impact of the mGlu(5)-positive allosteric modulator CDPPB. Brain Res. *1768*, 147577. https://doi.org/10.1016/j.brainres.2021.147577.

65. Desai, N.S., Cudmore, R.H., Nelson, S.B., and Turrigiano, G.G. (2002). Critical periods for experience-dependent synaptic scaling in visual cortex. Nat. Neurosci. *5*, 783–789. https://doi.org/10.1038/nn878.

66. Maffei, A., Nelson, S.B., and Turrigiano, G.G. (2004). Selective reconfiguration of layer 4 visual cortical circuitry by visual deprivation. Nat. Neurosci. *7*, 1353–1359. https://doi.org/10.1038/nn1351.

67. Maffei, A., Nataraj, K., Nelson, S.B., and Turrigiano, G.G. (2006). Potentiation of cortical inhibition by visual deprivation. Nature *443*, 81–84. https://doi.org/10.1038/nature05079.

68. Hengen, K.B., Lambo, M.E., Van Hooser, S.D., Katz, D.B., and Turrigiano, G.G. (2013). Firing rate homeostasis in visual cortex of freely behaving rodents. Neuron *80*, 335–342. https://doi.org/10.1016/j.neuron.2013.08.038.

69. Keck, T., Keller, G.B., Jacobsen, R.I., Eysel, U.T., Bonhoeffer, T., and Hübener, M. (2013). Synaptic scaling and homeostatic plasticity in the mouse visual cortex in vivo. Neuron *80*, 327–334. https://doi.org/10.1016/j.neuron.2013.08.018.

70. Lefort, S., Gray, A.C., and Turrigiano, G.G. (2013). Long-term inhibitory plasticity in visual cortical layer 4 switches sign at the opening of the critical period. Proc. Natl. Acad. Sci. USA *110*, E4540–E4547. https://doi.org/10.1073/pnas.1319571110.

71. Barnes, S.J., Franzoni, E., Jacobsen, R.I., Erdelyi, F., Szabo, G., Clopath, C., Keller, G.B., and Keck, T. (2017). Deprivation-induced homeostatic spine scaling in vivo is localized to dendritic branches that have undergone recent spine loss. Neuron *96*, 871–882.e5. https://doi.org/10.1016/j.neuron.2017.09.052.

72. Qiu, Z., Sylwestrak, E.L., Lieberman, D.N., Zhang, Y., Liu, X.Y., and Ghosh, A. (2012). The Rett syndrome protein MeCP2 regulates synaptic scaling. J. Neurosci. *32*, 989–994. https://doi.org/10.1523/JNEUROSCI.0175-11.2012.

73. Zhong, X., Li, H., and Chang, Q. (2012). MeCP2 phosphorylation is required for modulating synaptic scaling through mGluR5. J. Neurosci. *32*, 12841–12847. https://doi.org/10.1523/JNEUROSCI.2784-12.2012.

74. Blackman, M.P., Djukic, B., Nelson, S.B., and Turrigiano, G.G. (2012). A critical and cell-autonomous role for MeCP2 in synaptic scaling up. J. Neurosci. *32*, 13529–13536. https://doi.org/10.1523/JNEUROSCI.3077-12.2012.

75. Tatavarty, V., Torrado Pacheco, A., Groves Kuhnle, C., Lin, H., Koundinya, P., Miska, N.J., Hengen, K.B., Wagner, F.F., Van Hooser, S.D., and Turrigiano, G.G. (2020). Autism-associated Shank3 is essential for homeostatic compensation in rodent V1. Neuron *106*, 769–777.e4. https://doi.org/10.1016/j.neuron.2020.02.033.

76. Soden, M.E., and Chen, L. (2010). Fragile X protein FMRP is required for homeostatic plasticity and regulation of synaptic strength by retinoic acid. J. Neurosci. *30*, 16910–16921. https://doi.org/10.1523/JNEUROSCI.3660-10.2010.

77. Bülow, P., Murphy, T.J., Bassell, G.J., and Wenner, P. (2019). Homeostatic intrinsic plasticity is functionally altered in Fmr1 KO cortical neurons. Cell Rep. *26*, 1378–1388.e3. https://doi.org/10.1016/j.celrep.2019.01.035.

78. Ellingford, R.A., Panasiuk, M.J., de Meritens, E.R., Shaunak, R., Naybour, L., Browne, L., Basson, M.A., and Andreae, L.C. (2021). Cell-type-specific synaptic imbalance and disrupted homeostatic plasticity in cortical circuits of ASD-associated Chd8 haploinsufficient mice. Mol. Psychiatr. *26*, 3614–3624. https://doi.org/10.1038/s41380-021-01070-9.

79. Rocher, A.B., Gubellini, P., Merienne, N., Boussicault, L., Petit, F., Gipchtein, P., Jan, C., Hantraye, P., Brouillet, E., and Bonvento, G. (2016). Synaptic scaling up in medium spiny neurons of aged BACHD mice: a slow-progression model of Huntington's disease. Neurobiol. Dis. *86*, 131–139. https://doi.org/10.1016/j.nbd.2015.10.016.

80. Kim, J., and Alger, B.E. (2010). Reduction in endocannabinoid tone is a homeostatic mechanism for specific inhibitory synapses. Nat. Neurosci. *13*, 592–600. https://doi.org/10.1038/nn.2517.

81. Kreitzer, A.C., and Malenka, R.C. (2007). Endocannabinoid-mediated rescue of striatal LTD and motor deficits in Parkinson's disease models. Nature *445*, 643–647. https://doi.org/10.1038/nature05506.

82. Dogra, S., and Conn, P.J. (2022). Metabotropic glutamate receptors as emerging targets for the treatment of schizophrenia. Mol. Pharmacol. *101*, 275–285. https://doi.org/10.1124/molpharm.121.000460.

83. Tu, J.C., Xiao, B., Naisbitt, S., Yuan, J.P., Petralia, R.S., Brakeman, P., Doan, A., Aakalu, V.K., Lanahan, A.A., Sheng, M., and Worley, P.F. (1999). Coupling of mGluR/Homer and PSD-95 complexes by the Shank family of postsynaptic density proteins. Neuron *23*, 583–592. https://doi.org/10.1016/s0896-6273(00)80810-7.

84. Ronesi, J.A., Collins, K.A., Hays, S.A., Tsai, N.P., Guo, W., Birnbaum, S.G., Hu, J.H., Worley, P.F., Gibson, J.R., and Huber, K.M. (2012). Disrupted Homer scaffolds mediate abnormal mGluR5 function in a mouse model of fragile X syndrome. Nat. Neurosci. *15*, 431–440. S1. https://doi.org/10.1038/nn.3033.

85. Matosin, N., Fernandez-Enright, F., Lum, J.S., Engel, M., Andrews, J.L., Gassen, N.C., Wagner, K.V., Schmidt, M.V., and Newell, K.A. (2016). Molecular evidence of synaptic pathology in the CA1 region in schizophrenia. NPJ Schizophr. *2*, 16022. https://doi.org/10.1038/npjschz.2016.22.

86. Engmann, O., Hortobágyi, T., Pidsley, R., Troakes, C., Bernstein, H.G., Kreutz, M.R., Mill, J., Nikolic, M., and Giese, K.P. (2011). Schizophrenia is associated with dysregulation of a Cdk5 activator that regulates synaptic protein expression and cognition. Brain *134*, 2408–2421. https://doi.org/10.1093/brain/awr155.

87. Cai, Y.Q., Cai, G.Q., Liu, G.X., Cai, Q., Shi, J.H., Shi, J., Ma, S.K., Sun, X., Sheng, Z.J., Mei, Z.T., et al. (2006). Mice with genetically altered GABA transporter subtype I (GAT1) expression show altered behavioral responses to ethanol. J. Neurosci. Res. *84*, 255–267. https://doi.org/10.1002/jnr.20884.

88. Jordan, B.A., Fernholz, B.D., Boussac, M., Xu, C., Grigorean, G., Ziff, E.B., and Neubert, T.A. (2004). Identification and verification of novel rodent postsynaptic density proteins. Mol. Cell. Proteomics *3*, 857–871. https://doi.org/10.1074/mcp.M400045-MCP200.

89. Yu, Z., Wu, Y.J., Wang, Y.Z., Liu, D.S., Song, X.L., Jiang, Q., Li, Y., Zhang, S., Xu, N.J., Zhu, M.X., et al. (2018). The acid-sensing ion channel ASIC1a mediates striatal synapse remodeling and procedural motor learning. Sci. Signal. *11*, eaar4481. https://doi.org/10.1126/scisignal.aar4481.

90. Höfner, G., and Wanner, K.T. (2010). Using short columns to speed up LC-MS quantification in MS binding assays. J. Chromatogr. B Analyt. Technol. Biomed. Life Sci. *878*, 1356–1364. https://doi.org/10.1016/j.jchromb.2009.12.006.

## STAR★METHODS

### KEY RESOURCES TABLE

| REAGENT or RESOURCE | SOURCE | IDENTIFIER |
|---|---|---|
| **Antibodies** | | |
| GluA1 Antibody | Epitomics | Cat# 3861-1 |
| GluA2 Antibody | Epitomics | Cat# 3520-1 |
| GluN1 Antibody | R&D Systems | Cat# PPS011B |
| GluN2A Antibody | Millipore | Cat# 07-632 |
| GluN2B Antibody | Millipore | Cat# MAB5220 |
| Actin Antibody | Chemicon | Cat# MAB1501 |
| Goat × Rabbit IgG HRP | Millipore | Cat# AP132P |
| Rabbit × Goat IgG HRP | Millipore | Cat# AP106P |
| Goat × Mouse IgG HRP | Millipore | Cat# AP124P |
| **Chemicals, peptides, and recombinant proteins** | | |
| DAPI | Cell Signaling Technology | Cat# 4083 |
| NASPM | MedChemExpress | Cat# HY-12506 |
| CDPPB | TOCRIS | Cat# 3235 |
| WIN 55,212-2 | TOCRIS | Cat# 1038 |
| PTX | Sigma | Cat# R284556 |
| CNQX | Sigma | Cat# C239 |
| APV | Sigma | Cat# A5282 |
| DHPG | Sigma | Cat# D3689 |
| Gabazine | MedChemExpress | Cat# 104104-50-9 |
| NO-711 | TOCRIS | Cat# N142 |
| SNAP5114 | MedChemExpress | Cat# 157604-55-2 |
| TRIzol Reagent | Invitrogen | Cat# 10296028 |
| Power SYBR Green PCR Master Mix | Applied Biosystems | Cat# 4367659 |
| **Experimental models: Organisms/strains** | | |
| Mouse: C57BL/6J (B6/J) | Shanghai Laboratory Animal Center, Shanghai | N/A |
| Mouse: GAT1$^{-/-}$ | Shanghai Model Organisms Center, Inc. | N/A |
| **Deposited data** | | |
| All sequencing fastq files generated in this project | Gene Expression Omnibus | GEO: GSE211419 |
| **Software and algorithms** | | |
| Clampfit 10.5 | Molecular Devices | N/A |
| Image-ProPlus 6.0 software | Media Cybernetics | N/A |
| Origin 9.5 Software | OriginLab Corporation | N/A |
| pCLAMP 10.5 | Molecular Devices | N/A |
| Photoshop CC | Adobe | N/A |
| Illustrator | Adobe | N/A |
| EthoVision XT | Noldus | N/A |
| Leica CM 1950 cryostat | Leica Biosystems | N/A |

(*Continued on next page*)

*Continued*

| REAGENT or RESOURCE | SOURCE | IDENTIFIER |
|---|---|---|
| LSM-510 | Carl Zeiss | N/A |
| FEI Talos L120C | Thermo Fisher Scientific | N/A |
| KDS 310 | KD Scientific | N/A |
| ISO-Flex stimulus isolator | AMPI | N/A |
| ImageQuant LAS 4000mini | GE Healthcare Life Sciences | N/A |
| Other | | |
| microRNA Isolation Kit | Ambion | Cat# AM1561 |
| FastQuant RT Kit | Tiangen | Cat# KR103 |
| mRNA-seq Library Prep Kit | Vazyme | Cat# NR602-01 |
| FD Rapid Golgistain Kit | FD NeuroTechnologies | Cat# PK401 |

## RESOURCE AVAILABILITY

### Lead contact

Further information and any related requests should be directed to and will be fulfilled by the lead contact, Prof. Tian-Le Xu (xu-happiness@shsmu.edu.cn).

### Materials availability

This study did not generate new unique reagents.

### Data and code availability

All data needed to evaluate the conclusions of the present study are present in the main paper and/or the supplemental information. The sequencing data generated in this study are deposited to the NCBI GEO (accession number: GSE185538) and are publicly available. We used many publicly available algorithms and packages for the genome annotation and differential analysis, which are properly cited in the manuscript. This paper did not produce original code. Any additional information required for reanalyzing the reported data is available from the lead contact upon request.

## EXPERIMENTAL MODEL AND SUBJECT DETAILS

### Mice

Care of animals and experimental procedures were approved by the Animal Care and Use Committee of Shanghai Jiao Tong University School of Medicine (Policy Number DLAS-MP-ANIM. 01-05). $GAT1^{+/+}$ and $GAT1^{-/-}$ littermates (male, 3–5 weeks old, C57BL/6J background) were bred from the GAT1 heterozygous mice.[87] The C57BL/6J mice were purchased from the Shanghai Laboratory Animal Center at the Chinese Academy of Sciences (Shanghai, China). All mice were bred in specific pathogen-free laboratory animal facilities under standard conditions with temperatures of 21–23°C, 40–60% humidity, and a 12-h light/dark cycle with rodent chow and water provided *ad libitum*. Mice were used in a randomized order during experiments and the investigators were blind to the genotype. For the behavioral tests, mice were acclimated to the behavior rearing room for at least 1 week and were habituated to the behavior testing room at least 1 hr before tests. Experimental manipulations were performed during the light-on phase of the light/dark cycle, in accordance with the institutional guidelines.

## METHOD DETAILS

### Brain slice electrophysiology

#### *Whole-cell recording*

Mice were deeply anesthetized with 1% sodium pentobarbital and were subsequently decapitated. Brains were dissected quickly and were chilled in well-oxygenated (95% $O_2$/5% $CO_2$, v/v) ice-cold artificial cerebrospinal fluid (ACSF) containing the following (in mM): 125 NaCl, 2.5 KCl, 12.5 D-glucose, 1 $MgCl_2$, 2 $CaCl_2$, 1.25$NaH_2PO_4$, and 25 $NaHCO_3$ (pH 7.35–7.45). Sagittal brain slices (300-μm thick) containing regions of the dorsal striatum were cut with a vibratome (Leica VT1000S, Germany). Slices were allowed to recover for 1–2 hr at 30°C oxygenated ACSF. Then, one slice was transferred to the recording chamber where it was perfused

with oxygenated ACSF at a rate of 2–3 ml/min at 30°C. Whole-cell voltage-clamp recordings from MSNs were performed with the aid of an infrared differential-interference contrast microscope (BX51WI, Olympus) and an optiMOS camera (QImaging). MSNs constituted 95% of neurons in the striatum and were visually identified by their shape, volume, and electrophysiological properties. Whole-cell patch-clamp recordings were performed using an Axon 200B amplifier (Molecular Devices). Membranous currents were sampled and analyzed using a Digidata 1440 interface and a personal computer running Clampex and Clampfit software (Version 10, Axon Instruments). The resistance of the patch pipette was 3–5 MΩ. Recordings with access resistance below 20 MΩ and with a change in access resistance < 20% were included in the analysis.

### *Electrical stimulation-evoked inhibitory postsynaptic currents (eIPSCs)*

The eIPSCs were recorded from striatal MSNs. Patch pipettes were filled with a $Cs^+$-based solution containing (in mM): 132.5 Cs-gluconate, 17.5 CsCl, 2 $MgCl_2$, 0.5 EGTA, 10 HEPES, 2 $Na_2$-ATP, 5 QX-314, with pH adjusted to 7.3 with CsOH, and osmolarity was 280–290 mOsm. The stimulations were delivered through an ISO-Flex stimulus isolator (A.M.P.I.) with bipolar tungsten stimulating electrode (0.1-ms duration) placed in the dorsal striatum, to induce eIPSCs. The $GABA_A$R-mediated eIPSCs were induced by repetitive stimulations at 0.05 Hz. The patched MSNs were voltage-clamped at 0 mV.

### *Miniature inhibitory postsynaptic currents (mIPSCs)*

For recording mIPSCs in striatal neurons, the holding potential was –70 mV. Patch pipettes were filled with an intracellular solution that contained the following (in mM): 140 KCl, 5 NaCl, 2 Mg-ATP, 0.3 $Na_2$-GTP, 0.1 EGTA, 10 HEPES. The pH was adjusted to 7.2, and the osmolarity was 300–310 mOsm. To isolate mIPSCs, tetrodotoxin (TTX, 0.5 μM), CNQX (20 μM), and APV (50 μM) were added to the ACSF to block action potential and glutamatergic responses.

### *Tonic GABA currents*

Tonic $GABA_A$R-mediated currents were recorded similarly to mIPSCs but without TTX, instead picrotoxin (PTX, 100 μM), CNQX (20 μM) and APV (50 μM) were applied. The tonic GABA currents were measured as the outward shift in the holding current.

### *Electrical stimulation-evoked excitatory postsynaptic currents (eEPSCs)*

To evoke glutamatergic synaptic responses in corticostriatal pathways, the stimulating electrode was placed in the corpus callosum, located between the medial prefrontal cortex and dorsal striatum, about 200–500 μm away from the recoded cell. Patch pipettes were filled with a $Cs^+$-based solution containing (in mM): 132.5 Cs-gluconate, 17.5 CsCl, 2 $MgCl_2$, 0.5 EGTA, 10 HEPES, 2 $Na_2$-ATP, 5 QX-314, with pH adjusted to 7.3 by CsOH, and the osmolarity was 280–290 mOsm. To determine the paired-pulse ratios (PPRs), the patched MSNs were voltage-clamped at –70 mV. We chose an electrical stimulus intensity approximately 70 μA that typically induces a current amplitude between 300–500 pA. The AMPAR-mediated eEPSCs were evoked by paired electrical stimulation (25-, 50-, 100-, 200-, and 500-ms intervals; 0.1-ms duration) at the corpus callosum and PPRs were calculated as the peak amplitude ratio of the second to the first eEPSC. The AMPAR- and NMDAR-mediated eEPSCs at different electrical stimulation intensities (by incremental increases of stimulation strength, from 10 to 70 μA, in 10-μA increments) were recorded. AMPAR-mediated eEPSCs were recorded in the presence of PTX at –70 mV; NMDAR-mediated eEPSCs were recorded in the presence of CNQX and PTX at +40 mV. To determine the AMPAR/NMDAR ratios, the AMPAR-mediated eEPSCs were recorded in the presence of PTX at –70 mV while the NMDAR-mediated eEPSCs were recorded in the presence of CNQX and PTX at +40 mV, with the electrical stimulation of the same intensity and duration. To determine homomeric-GluA1 AMPAR mediated eEPSCs, we inhibited homomeric-GluA1-AMPARs with 1-naphthylacetyl spermine (NASPM, 50 μM), a selective CP-AMPAR antagonist, for 10 min. The amplitude of eEPSCs inhibited by NASPM was taken as homomeric-GluA1 AMPAR mediated eEPSCs. To determine the DHPG-dependent LTD in the corticostriatal pathways, AMPAR mediated eEPSCs of MSNs were evoked by paired electrical stimulations (50-ms interval; 0.1-ms duration) and recorded for 10 min as the baseline, continuously recorded for another 10 min after DHPG (50 μM) application, and at last, recorded for 30 min after the washout of DHPG. The amplitude of the first peaks and PPRs were analyzed.

### *Miniature excitatory postsynaptic currents (mEPSCs)*

For recording mEPSCs in striatal neurons, the holding potential was –70 mV. Patch pipettes were filled with a $Cs^+$-based solution containing (in mM): 132.5 Cs-gluconate, 17.5 CsCl, 2 $MgCl_2$, 0.5 EGTA, 10 HEPES, 2 $Na_2$-ATP, 5 QX-314, with pH adjusted to 7.3 by CsOH, and the osmolarity was 280–290 mOsm. TTX and gabazine (20 μM) were added in the ACSF to isolate mEPSCs. The mEPSCs were recorded for 20 min and analyzed from 200–300 s after the establishment and stabilization of the recording. Data were analyzed using the Mini-analysis Program (Synaptosoft) with an amplitude threshold of 10 pA while other parameters were the default values.

## Western blotting

To determine the expression and allocation of glutamate receptors, striatal total protein lysates and PSD (postsynaptic density) components were collected from the adolescent $GAT1^{+/+}$ and $GAT1^{-/-}$ littermates. To prepare striatal total protein samples from brain tissues, mice were killed by cervical dislocation and their striata were dissected, homogenized, and lysed on ice for 30 min. The lysis buffer used for protein extraction contained (in mM): 150 NaCl, 1% Triton X-100, 1 EDTA, 3 NaF, 1 β-glycerophosphate, 1 $Na_3VO_4$, 10% glycerol, and 20 Tris-Cl, pH 7.4, supplemented with protease inhibitors and phosphatase inhibitors. The lysates were centrifuged at 13,000 × g for 15 min at 4°C and the supernatants were collected. Then, SDS-PAGE loading buffer was added to the collected supernatants and the samples boiled for 5 min. The purification of PSD fractions was performed based on previous studies.[88,89] Briefly, striatal tissue samples combined from 4 mice were homogenized in a buffer containing (in mM): 1 $MgCl_2$, 0.5 $CaCl_2$, and 5 HEPES, pH 7.4, in the presence of protease inhibitors and phosphatase inhibitors. The homogenate was centrifuged at 1,400 × g for 10minat 4°C. The resulting supernatant (S1) was saved and the pellet was resuspended and centrifuged at 700 × g. The resulting supernatant (S1′) was combined with S1 and the mixture centrifuged at 13,800 × g for 10minat 4°C to obtain a crude membrane fraction in the pellet (P2 fraction). The P2 fraction was resuspended in 0.32 M sucrose, loaded onto a discontinuous sucrose gradient (from the top, 0.85 M: 1.0 M: 1.2 M = 3 ml: 3 ml: 3 ml), and then centrifuged at 82,500 × g for 2hrat 4°C using an SW-41 rotor (Beckman Coulter, USA). The synaptosome fraction between 1 M and 1.2 M sucrose was collected with a syringe needle and resuspended in a buffer containing 6 mM Tris (pH 8.1) and 0.5% Triton X-100. After 15 min treatment by Triton X-100 at 4°C, the suspension was centrifuged at 201,800 × g using a Type 90 Ti rotor (Beckman Coulter, USA) for 1 hr at 4°C and the final pellet (PSD) was resuspended with a buffer containing 0.2% SDS. The "One-Triton" PSD was used because of the limit in the amount of starting materials. PSD proteins were highly enriched in our preparations, in which presynaptic components, indicated by synaptophysin, were nearly absent (data not shown). The PSD proteins were dissolved in the lysis buffer to lyse for 20 min, which was followed by the addition of the SDS-PAGE loading buffer.

Protein samples from striatum or purified PSD were separated by 7% SDS-PAGE and transferred to polyvinylidene difluoride filters. The filters were incubated overnight at 4°C with appropriate antibodies, then incubated with secondary antibodies at room temperature for 2 hr. All the primary antibodies used in our current manuscript has been validated by many publications with Western-blotting techniques in mice. Antibodies used in this study were as follows: GluA1 (1:2000; Epitomics, USA; Cat# 3861-1), GluA2 (1:1000; Epitomics, USA; Cat# 3520-1), GluN1 (1:1000; R&D Systems, USA; Cat# PPS011B), GluN2A (1:2000; Millipore, USA; Cat# 07-632), GluN2B (1:500; , Millipore, USA; Cat# MAB5220), and β-actin (1:2000; Chemicon, USA; Cat# MAB1501). The secondary antibodies were from Millipore (1:1000). The visualization was performed *via* the ImageQuant LAS 4000 mini–Molecular Imaging System (GE Healthcare Life Sciences, USA), and Quantity One was used for the analysis of optic density. The experiments were repeated at least 6 times per group.

## Electron microscopy (EM) and Golgi-Cox staining

### *Electron microscopy*

Adolescent $GAT1^{+/+}$ and $GAT1^{-/-}$ mice were perfused transcardially with saline, followed by ice-cold mixture of 2% PFA and 0.1% glutaraldehyde (GA) in 0.1M PB (pH 7.4). Brains were dissected out and post-fixed at 4°C. One day later, the dorsal striatum was separated. Then EM samples were prepared at the Electron Microscopy Facility of Shanghai Jiao Tong University School of Medicine. Images were acquired at a 28,000-magnification using the FEI Talos L120C (Thermo Fisher Scientific, USA). Ultrastructural synapses were defined by postsynaptic densities with closely apposed presynaptic boutons filled with synaptic vesicles. The measurements of striatal PSD thickness and length were performed using

Image-ProPlus 6.0 software (Media Cybernetics, USA) by an observer who was blind to the genotypes of the samples.

### *Golgi-Cox staining*

Golgi-Cox staining was performed using an FD Rapid Golgistain Kit (FD NeuroTechnologies, USA). Briefly, unfixed GAT1$^{+/+}$ and GAT1$^{-/-}$ mouse brains were rapidly removed, washed in distilled water, and immersed in the impregnation solutions according to the manufacturer's instructions. Then the brains were cut into coronal sections (100 μm) on a Leica CM 1950 cryostat (Leica Biosystems, Germany) and mounted on gelatin-coated microscope slides. After drying at the room temperature (22–24°C), sections were stained, rinsed, dehydrated, cleared, and covered with cover glasses in a permount mounting medium. The progress was completed in the dark. Sections were selected between bregma 1.10 mm and 0.38 mm and then analyzed using a Zeiss LSM-510 confocal microscope (Carl Zeiss, Germany). Confocal z-stacks of MSN dendritic segments were acquired with a 63 × oil immersion objective at 0.8 μm intervals. For each genotype, a total of 50–60 images were captured from the dorsal striata of 3 different mice. Dendritic spine morphology (spine density, spine head width) was analyzed with the Image-ProPlus 6.0 software (Media Cybernetics, USA). The measurements were made from secondary dendrites which were 50–70 μm distal to the cell soma.

## Surgical procedures and drug delivery

### *Surgical procedures*

Before the surgery, the adolescent GAT1$^{+/+}$ and GAT1$^{-/-}$ mice were anesthetized and fixed on a stereotaxic device (RWD Life Science, China). The surface of the skull was exposed, and small holes were drilled above the dorsal striatum using the following stereotaxic coordinates: AP, +0.4 mm; ML, ±3.3 mm; DV, –3.2 mm, with a mediolateral angle at 20 degrees. Stainless-steel guide cannulas (33 gauges, RWD Life Science, China) were implanted bilaterally in the dorsal striatum through the holes and secured with dental acrylic. Mice were allowed to recover for at least 1 week before behavioral tests. After completing all the tests, the mice were perfused with fixative to confirm the accurate locations of the cannulas.

### *Drug delivery*

During drug infusions, mice were briefly head-restrained, while the stainless-steel obturators were removed and injection cannulas were inserted into the guide cannulas. Injection cannulas protruded 0.5 mm from the tips of guide cannulas. Infusion cannulas were connected via PE20 tubing to a microsyringe driven by a microinfusion pump (KDS 310, KD Scientific, USA). NASPM (50 nM in ACSF, 0.8 μl per side) were infused bilaterally into the target brain areas at a flow rate of 0.2 μl per min. After finishing drug injections, the injection cannulas were left in place for 2 min to allow the solution to diffuse from each cannula tip. The stainless-steel obturators were subsequently reinserted into guide cannulas and the mice returned to their home cage for 30 min before open field tests. Vehicle control groups received the infusions of 0.8 μl ACSF. To strengthen the effect of genetic disruption of GAT1 on homeostatic excitatory synaptic scaling and the associated locomotor hyperactivity, we fed weaned wild type mice (3 weeks) with water containing 0.025 mg/ml NO-711 to achieve an approximately 2.5 mg/kg per day dosing, which lasted for 10 days. To pharmacologically potentiate mGluR-eCB signaling *in vivo*, WIN 55,212-2 mesylate (1 mg/kg, TOCRIS, USA) and CDPPB (3 mg/kg, TOCRIS, USA) were injected intraperitoneally (i.p.). About 30 min after the injection, animals were placed into the arena for observing their locomotor activity.

## Open field test

The behavioral tests were done in the experimental room. Mice in their home cages were transferred to the experimental room and habituated there for at least 1 hr before the experiment. To test the effects of drugs, 30 min after the injection, mice were placed in the center of a square Plexiglas open field apparatus (40 × 40 × 35 cm) and allowed to freely explore for 30 min. The open-field arena was thoroughly cleaned with 70% ethanol between each test. The total distance traveled was quantified using the EthoVision video tracking system (Noldus Information Technology, Netherlands).

## RNA sequencing

Dorsal striatal samples from three GAT1$^{+/+}$ and three GAT1$^{-/-}$ mice were pulled for RNA sequencing. Total RNA was extracted using a mirVana miRNA Isolation kit (Cat# AM1561, Thermo Fisher Scientific, USA) following the manufacturer's instructions. The quantification and integrity of the RNA samples obtained

were determined using Qubit 2.0 Fluorometer (Thermo Fisher Scientific, USA) and Agilent Bioanalyzer 2100 (Agilent Technologies, USA), respectively. Only samples with RNA integrity numbers of > 8 (out of 10) were used for sequencing. Samples were prepared for sequencing by Shanghai Biotechnology Corporation using the VAHTS Stranded mRNA-seq Library Prep Kit for Illumina (Vazyme, China) and barcoded to allow samples to be multiplexed within a flow cell lane. Barcoded complementary DNA (cDNA) libraries were sequenced on a single lane of the Illumina HiSeq X Ten Sequencing System to obtain 150-base pair (bp) single-end reads at an approximate sequencing depth of 25.6 to 30.3 million reads per sample. Raw reads were trimmed to remove sequencing artifacts (1 bp from 3' end) and filtered to remove low-quality reads (reads with quality scores of < 20 in more than 10% of bases) before alignment to the mouse genome (mm10) using HISAT2 (version 2.0.4). Differential expression analysis was conducted with edgeR, which was used to quantify transcript reads and to obtain z scores and fold change values for individual genes. Genes with a corrected *p*-value of $\leq$0.05 (Benjamini-Hochberg FDR correction) and fold change of $\geq$1.5 were selected for further analysis. Gene ontology categories were manually curated from the results.

### Quantitative real-time PCR

The dorsal striatal tissues from GAT1$^{+/+}$ and GAT1$^{-/-}$ mice were collected and rapidly frozen in liquid nitrogen. The total RNA was extracted from the striatal tissues using TRIzol Reagent (Thermo Fisher Scientific, USA). Four micrograms of total RNA were used as a template for cDNA synthesis and amplification with the FastQuant RT Kit (Tiangen, China) according to the manufacturer's instructions. The cDNA was diluted to an equal concentration of 400 ng/μl, and 80 ng of which was used for further PCR amplification. Real-time PCR was then performed using the cDNA as a template in a Power SYBR Green PCR Master Mix (Thermo Fisher Scientific, USA). The primers used were as follows:

Gapdh, 5'-CCTCGTCCCGTAGACAAAATGGT-3' (forward),

and 5'-TTGAGGTCAATGAAGGGGTCGT-3' (reverse);

Grm1, 5'-GAGGCCATGTTCCACACATTA-3' (forward),

and 5'-CCAGCAATAGGCTTCTTAGTCCT-3' (reverse);

Grm2, 5'-GCTCCCACAGCTATCACCG-3' (forward),

and 5'-TCATAACGGGACTTGTCGCTC-3' (reverse);

Grm3, 5'-CTGGAGGCCATGTTGTTTGC-3' (forward),

and 5'-TGTACGAACCGCCAATGACTC-3' (reverse);

Grm4, 5'-CCCATACCCATTGTCAAGTTGG-3' (forward),

and 5'-TGTAGCGCACAAAAGTGACCA-3' (reverse);

Grm5, 5'-GCTGTGAGATAAGAGATTCCTGC-3' (forward),

and 5'-ACTCCCACTATGGGTTTCTTGG-3' (reverse);

Grm6, 5'-GTCCATCATGGTCGCCAATGT-3' (forward),

and 5'-AGTCATAGCGTGTGGAGTCAC-3' (reverse);

Grm7, 5'-CTCCGCGTCCTGACTTTGATG-3' (forward),

and 5'-TCTGGTCGAGAGCATAAAGCATA-3' (reverse);

Grm8, 5'-CAGACTTGAGGCCATGCTTTA-3' (forward),

and 5′-CCGGACACCCAGAGTGATATT-3′ (reverse);

Homer1, 5′-GACGATGAGAGAACACCCGA-3′ (forward),

and 5′-GAGGAGCTCTCCAGCAAAGAA-3′ (reverse);

Homer1a, 5′-CAAACACTGTTTATGGACTG-3′ (forward),

and 5′-TGCTGAATTGAATGTGTACC-3′ (reverse);

Homer1b/c, 5′-AGAGCTGAACCAGACAGTGC-3′ (forward),

and 5′-GGTTACTGCGGAAAGCCTCT-3′ (reverse);

Abhd4, 5′-GCAGGGCTTGTTTACTATGGCT-3′ (forward),

and 5′-CTTGTTCTGGTTTGGGAGGGA-3′ (reverse);

Cn1r, 5′-TCTCATAGAGTCTGGGGGCAA-3′ (forward),

and 5′-CAGGCTCAACGTGACTGAGA-3′ (reverse);

Daglα, 5′-AGTACGTGCTCTACGTGCG-3′ (forward),

and 5′-GCAGAGGACAGTGATGCAGA-3′ (reverse);

Daglβ, 5′-CTGACGTTGTATCTCACGCAC-3′ (forward),

and 5′-ATAGACTTCCGAGGTCCAGG-3′ (reverse);

Gde1, 5′-GGCCATGCAGATATGGCTTCT-3′ (forward),

and 5′-GCCTGTGAGTTAGGGCTGTG-3′ (reverse);

Napepld, 5′-ACCGCGGTTCCTTTTCGTT-3′ (forward),

and 5′-TCGGCGAGAAGTCGAAACC-3′ (reverse);

Faah, 5′-CATGGCACGGGATGTGGATA-3′ (forward),

and 5′-GTATCCCACACGAAGGGGTC-3′ (reverse).

The plate was run in the Applied Biosystems 7500 Fast Real-Time PCR System under the Standard 7500 run mode (one cycle 50.0°C, 20 s; one cycle 95.0°C, 10 min; 35 cycles 95.0°C, 15 s, and 60°C, 1 min with fluorescence measured during the 60°C steps). Data were then analyzed using the $2^{-\triangle\triangle Ct}$ method. All collected data were normalized to the $GAT1^{+/+}$ group.

### Liquid chromatograph mass spectrometer

Mice were given a two-day water abstinence, and after feeding water with NO-711 (0.025 mg/ml) for 1 hr, brain tissues were collected and the concentration of NO-711 was determined by high performance liquid chromatography-mass spectrometry (LC-MS). LC effectively separated the NO-711 in the sample, while MS analyzed the concentration (quantitative analysis). LC-MS analysis was performed directly from the matrix produced by the binding assay.[90]

## QUANTIFICATION AND STATISTICAL ANALYSIS

No statistical methods were used to predetermine sample sizes, but the sample sizes used are similar to those generally employed in the field. The data were collected and processed randomly. Experimenters

were blind to the genotype and pharmacological treatment until all data were collected and analyzed. Data distributions were tested for normality and variance equality among groups was assessed using Levene's test. No data points were excluded. Most histograms display individual data points that represent the values and numbers of individual samples for each condition. Data are presented as the mean ± the standard error of the mean (S.E.M.) unless indicated otherwise. All statistical analyses were performed using IBM SPSS Statistics 25 (SPSS). Unpaired Student's t-test, one-way ANOVA test followed by Fisher's LSD test, two-way ANOVA followed by Dunnett's T3 post-hoc test and two-sample Kolmogorov-Smirnov test were used for comparisons as mentioned in Figure legends. $p < 0.05$ was considered to be significantly different. Not significant values are not denoted except for emphasis.